

 Open access • Posted Content • DOI:10.1101/2020.07.09.193847

Phage-delivered CRISPR-Cas9 for strain-specific depletion and genomic deletions in the gut microbiota — [Source link](#)

Kathy N. Lam, Peter Spanogiannopoulos, Paola Soto-Perez, Margaret Alexander ...+4 more authors

Institutions: University of California, San Francisco

Published on: 09 Jul 2020 - bioRxiv (Cold Spring Harbor Laboratory)

Topics: Microbiome, Gut flora, Bacteriophage, Escherichia coli and CRISPR

Related papers:

- [Transfer and Persistence of a Multi-Drug Resistance Plasmid in situ of the Infant Gut Microbiota in the Absence of Antibiotic Treatment.](#)
- [In Vivo Targeting of Clostridioides difficile Using Phage-Delivered CRISPR-Cas3 Antimicrobials.](#)
- [Stable Neutralization of a Virulence Factor in Bacteria Using Temperate Phage in the Mammalian Gut.](#)
- [Stable neutralization of virulent bacteria using temperate phage in the mammalian gut](#)
- [The enemy from within: a prophage of Roseburia intestinalis systematically turns lytic in the mouse gut, driving bacterial adaptation by CRISPR spacer acquisition](#)

Share this paper:    

View more about this paper here: <https://typeset.io/papers/phage-delivered-crispr-cas9-for-strain-specific-depletion-4qnqtp9bes>

Phage-delivered CRISPR-Cas9 for strain-specific depletion and genomic deletions in the gut microbiota

Kathy N. Lam¹, Peter Spanogiannopoulos¹, Paola Soto-Perez¹, Margaret Alexander¹,
Matthew J. Nalley¹, Jordan E. Bisanz¹, Feiqiao B. Yu², Peter J. Turnbaugh^{1,2,*}

¹ Department of Microbiology and Immunology, University of California San Francisco, USA

² Chan-Zuckerberg BioHub, San Francisco, USA

* Correspondence to: Peter.Turnbaugh@ucsf.edu

Abstract

The recognition that the gut microbiome has a profound influence on human health and disease has spurred efforts to manipulate gut microbial community structure and function. Though various strategies for microbiome engineering have been proposed, methods for phage-based genetic manipulation of resident members of the gut microbiota *in vivo* are currently lacking. Here, we show that bacteriophage can be used as a vector for delivery of plasmid DNA to bacteria colonizing the gastrointestinal tract, using filamentous phage M13 and *Escherichia coli* engrafted in the gut microbiota of mice. We employ M13 to deliver CRISPR-Cas9 for sequence-specific targeting of *E. coli* leading to depletion of one strain of a pair of fluorescently marked isogenic strains competitively colonizing the gut. We further show that when mice are colonized by a single *E. coli* strain, it is possible for M13-delivered CRISPR-Cas9 to induce genomic deletions that encompass the targeted gene. Our results suggest that rather than being developed for use as an antimicrobial in the gut microbiome, M13-delivered CRISPR-Cas9 may be better suited for targeted genomic deletions *in vivo* that harness the robust DNA repair response of bacteria. With improved methods to mitigate undesired escape mutations, we envision these strategies may be developed for targeted removal of strains or genes present in the gut microbiome that are detrimental to the host. These results provide a highly adaptable platform for *in vivo* microbiome engineering using phage and a proof-of-concept for the establishment of phage-based tools for a broader panel of human gut bacteria.

Introduction

Broad interest in the influence that the gut microbiome has on host health and disease has led to the development of strategies with which to manipulate the structure and function of host-associated microbial communities. Various approaches for microbiome modification have recently been described, including engrafting bacterial strains in a naive host by providing exclusive nutrient sources in the diet [1, 2] or treating with antibiotics [3, 4]; introducing transient bacteria as a live therapeutic to complement an absent host metabolic activity [5, 6]; and chemically inhibiting microbial pathways active in host disease states [7] or drug-induced toxicity [8]. Bacteria have also been engineered to respond *in vivo* (within the gut) to dietary compounds and synthetic inducers [9, 10], as well as to deliver genetic payloads to diverse members of the gut microbiota [11] or to target multi-drug resistant opportunistic pathogens [12]. Current strategies for microbiome editing, however, either lack species- or strain-level precision or require the introduction of an exogenous bacterium into the host. A valuable and complementary strategy is the genetic manipulation of members of the gut using more specific tools to target bacteria for genome modification *in vivo*.

Although bacterial viruses (bacteriophage or phage) have a long history of use in phage therapy [13–17], these applications have generally focused on the clearance of bacterial pathogens and made use of phages in their native form. In the case of *E. coli*, the use of coliphages to target the bacterium in the gut of mice suggested that eradication or permanent depletion may be complicated by factors that include the emergence of phage resistance, protective effects of the gut environment that allow phage-sensitive cells to persist, or changes in bacterial physiology that may impact phage infection *in vivo* [18–21]. An example of the latter are the phase-variable capsules of the gut bacterium *Bacteroides thetaiotaomicron* that lead to varying phage susceptibilities [22]. More recently, the discovery of CRISPR-Cas (endonuclease-containing systems able to generate

breaks in nucleic acid at targets defined by CRISPR guide sequences) has enabled the
engineering of phage programmed to cleave the DNA of pathogens. For example, engineered
phage carrying CRISPR-Cas9 have been used in models of infection for sequence-specific
targeting of enterohemorrhagic *E. coli* in moth larvae and antibiotic-resistant *Staphylococcus*
aureus on mouse skin [23–25]. Engineered phage carrying only the CRISPR guide sequences
have also been used against pathogenic *C. difficile* in the mouse gut and function by hijacking the
bacterium’s endogenous CRISPR-Cas3 system [26]. The sheer diversity of phages existing in
nature, the ease with which they can be isolated against a wide range of bacteria, and their natural
abundance [27, 28] make them attractive agents to engineer for gene delivery to bacterial cells
colonizing the gut. Despite the huge potential of phages in this respect, there is currently a lack of
in vivo models with which to study genetically tractable pairs of phages and their bacterial hosts
specifically in the context of genetic editing of a commensal microbe within an established
host-associated microbial community. Given the complexities and challenges of the mammalian gut
environment, the possibility of harnessing phage and CRISPR-Cas9 for gut microbiome editing
may be best explored with highly controlled, molecular mechanistic experiments using a
reductionist tripartite model system of *E. coli*, a coliphage, and mouse model [29].

Isolated nearly six decades ago from wastewater [30], M13 is a ssDNA filamentous phage
belonging to the Inoviridae family in the ICTV classification of viruses [31] and has an interesting
life cycle in which it replicates and releases new virions from the cell without causing lysis [32]. It
can infect *E. coli* and related Enterobacteriaceae carrying the F sex factor that encodes proteins
forming the conjugative F pilus (strains designated as F+, F', or Hfr) [33, 34]. M13 has made
impressive contributions to the field of molecular biology — from the development of M13-based
vectors for cloning, sequencing, and mutagenesis [35–37] to its application in phage
display [38, 39] — making it a very well characterized phage with excellent resources. In particular,

the development of phagemid vectors that have both a plasmid origin of replication and an origin 66
for packaging by M13 (*e.g.*, ColE1 and f1, respectively) combine the advantages of plasmid DNA 67
manipulation using standard techniques with the ability to easily package recombinant DNA into 68
virions and generate phage preparations of high titer. Furthermore, the recent appreciation that 69
inoviruses are prevalent in nature and have phylogenetically diverse hosts [40] suggests that M13 70
could be a useful model for extending to other bacterial species in the gut. 71

Phage M13 has been used previously in mice; for example, phage-displayed random peptide 72
libraries have been screened in mice to identify “homing” peptides able to target organs or 73
tumours [41–43]. M13 has also been applied by intraperitoneal injection as a bactericidal agent 74
against *E. coli* by engineering it to deliver constructs that encode toxins lethal to the cell [44] or 75
suppressors of the cellular response to DNA damage to enhance the efficacy of bactericidal 76
antibiotics [45]. Of relevance to the gut microbiome, M13 phage displaying antibody variable 77
fragments against *Helicobacter pylori* surface antigens have been shown to reduce colonization by 78
the bacterium in the mouse stomach when bacteria are pretreated with phage before oral 79
inoculation [46], and M13 carrying CRISPR-Cas9 have been used as an antimicrobial in a larval 80
model of bacterial infection [23]. However, the use of M13 to deliver genetic constructs to 81
established cells in the complex environment of the mammalian gastrointestinal tract for 82
maintenance in the host has not been demonstrated, nor has its use as phage chassis for delivery 83
of a CRISPR-Cas system to cells residing in the mouse gut. Here, we employ the established 84
streptomycin-treated mouse model to stably engraft *E. coli* among the microbiota [4, 47–49] and 85
demonstrate that M13 can be used to deliver phagemid DNA to *E. coli* cells in the mouse gut, and 86
further apply this strategy to deliver phagemid vectors carrying CRISPR-Cas9 to manipulate strain 87
composition as well as the genomic content of cells *in vivo*. 88

Results

89

Phage M13 can be used to deliver DNA to *E. coli* in the gut

90

To test whether we could deliver plasmid DNA via M13 to *E. coli* colonizing the gut, we turned to the existing phagemid pBluescript II [50]. We made use of the *bla* gene (encoding beta-lactamase) carried on this vector, which confers resistance to beta lactam antibiotics, reasoning that successful delivery to *E. coli* in the gut could be selected for using a beta-lactam in the drinking water of mice. Previous studies on the fate of orally administered antibiotics in animals showed that the beta lactam antibiotic ampicillin is poorly absorbed in the small intestine leading to the majority of the drug entering the cecum of rats and large intestine of lambs [51, 52], that resistant strains could be selected for when the antibiotic was provided [53, 54], and that mice will tolerate a concentration of 1 mg/ml in the water [55]. We determined that pBluescript II confers *in vitro* resistance to ampicillin and the semi-synthetic analogue carbenicillin at concentrations exceeding 1 mg/ml while sensitive strains displayed growth inhibition at concentrations 1 to 2 orders of magnitude lower (Figure S1).

91

92

93

94

95

96

97

98

99

100

101

To determine whether a resistant subpopulation could be selected for in the gut using a beta-lactam antibiotic in the water, we turned to the streptomycin-treated mouse model; although streptomycin treatment decreases bacterial diversity (Figure S2), it remains a useful model for experimentation with *E. coli* in the mammalian gut. We put mice on water containing streptomycin to prepare for colonization, and subsequently introduced a Sm^R *E. coli* population that was a mixture of 99.9% Amp^S (no plasmid) and 0.1% Amp^R cells (pBluescript II); mice were then split into 2 groups and maintained on water containing only streptomycin (5 mg/ml) or streptomycin and ampicillin (5 mg/ml and 1 mg/ml, respectively) (Figure 1a). We tracked both total *E. coli* and Amp^R *E. coli* in mouse feces for 8 days. At 6 hours post-*E. coli* introduction, the percentage of Amp^R *E. coli* in the feces of all mice was at or close to 0.1%, consistent with the gavaged mixture transiting through the

102

103

104

105

106

107

108

109

110

111

gastrointestinal (GI) tract. Within 1 to 2 days, however, mice on water containing ampicillin 112
exhibited an increase in the percent of Amp^R *E. coli* by 3 orders of magnitude, reaching complete 113
or near complete colonization by Amp^R cells, whereas the Amp^R subpopulation was lost in mice 114
treated with water containing only streptomycin (Figure 1a). These results demonstrate that a beta 115
lactam antibiotic can be used in the drinking water to select for resistant *E. coli* in combination with 116
the streptomycin model without impacting overall *E. coli* colonization levels, which are very 117
reproducible in this system averaging 10⁹–10¹⁰ CFU per gram feces (Figure 1a). 118

After confirming that beta lactam-resistant *E. coli* could be selected for using antibiotic in the 119
drinking water, we next wanted to determine how effective beta lactam selection was against a 120
sensitive population of *E. coli*— that is, whether selection could eradicate *E. coli* that had 121
established stable colonization in the mouse gut. A previous study found that a single high dose of 122
ampicillin effected a decrease in the resident sensitive *E. coli* from 10⁸–10⁹ to 10⁵–10⁶ CFU per 123
gram feces [52] while another study reported the emergence of spontaneous resistant mutants of 124
E. coli under ampicillin selection *in vivo* [56]. Because either of these two scenarios — a high 125
background of sensitive cells or the emergence of spontaneous resistant mutants — could 126
potentially hinder our strategy of using phage to deliver constructs to cells in the gut, we asked 127
whether they could occur in our system. To determine the effectiveness of beta lactam selection 128
against sensitive *E. coli*, we colonized mice with two different Sm^R strains (*E. coli* MG1655 and 129
W1655 F+) and tracked colonization levels during treatment with the beta lactam antibiotic 130
carbenicillin in an alternating exposure regimen lasting 17 days (Figure 1b); carbenicillin was used 131
here and all subsequent experiments for its increased stability over ampicillin. When colonized 132
mice were introduced to carbenicillin (1 mg/ml) in the drinking water, *E. coli* levels dropped 6 to 7 133
orders of magnitude from 10⁹–10¹⁰ to 10³–10⁴ CFU per gram feces in the first day, and levels 134
decreased to below the limit of detection (approximately 10² CFU per gram) over the course of 135

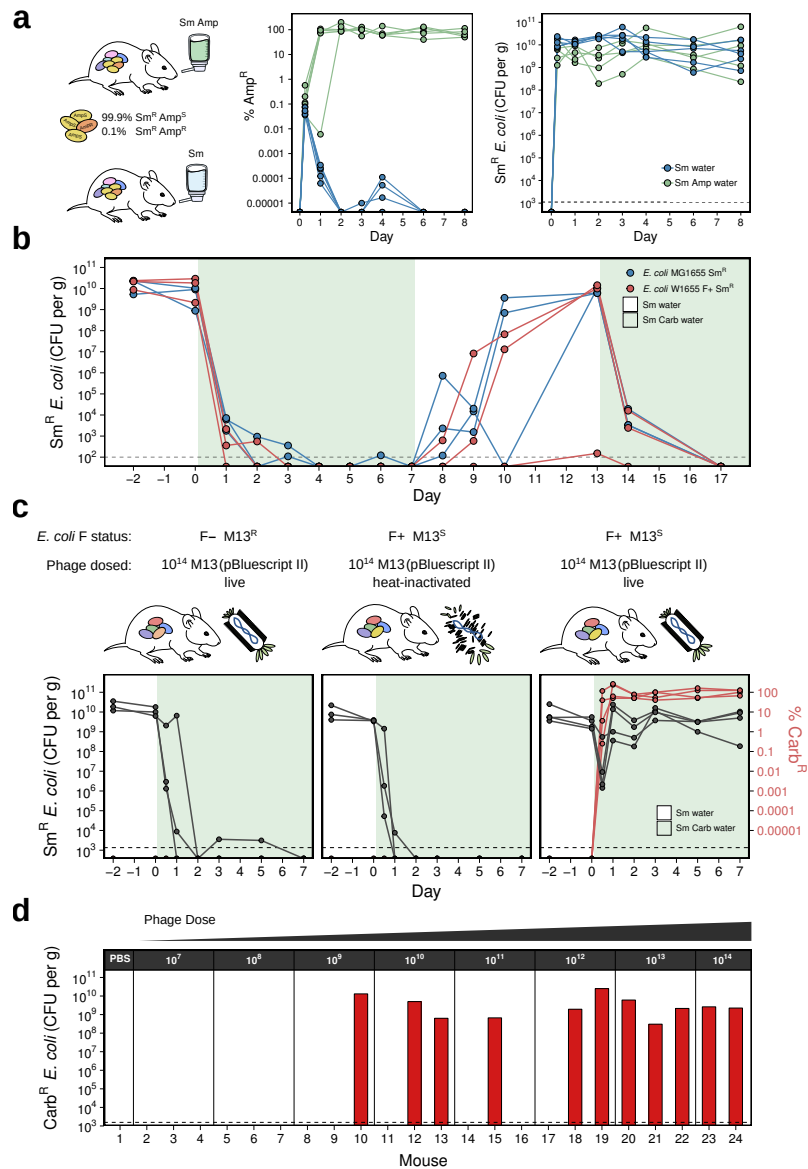


Figure 1. M13 phage can deliver a plasmid-borne antibiotic resistance gene to *E. coli* cells in the mouse gut using the streptomycin treatment model for engrafting *E. coli* in mice. (a) A resistant subpopulation of *E. coli* can be selected for in the gut when a beta lactam antibiotic is provided in the drinking water. Mice were orally gavaged with a mixture of Sm^R *E. coli* MG1655 containing 99.9% Amp^S cells and 0.1% Amp^R cells (Amp^R conferred by the plasmid pBluescript II). Mice were then started on water containing only streptomycin (n = 5) or water containing both streptomycin and ampicillin (n = 6). Percent Amp^R and total *E. coli* in mouse fecal pellets were determined on MacConkey agar with antibiotic selection. **(b)** A sensitive *E. coli* population is unable to maintain colonization in the gut when the beta lactam antibiotic carbencillin is provided in the water. Mice were colonized with either Sm^R MG1655 or Sm^R W1655 F+ (n = 3 per strain) using streptomycin in the water. Carbencillin was added to the water on Day 0, removed on Day 7, and added again on Day 13. Sm^R CFU per gram feces was determined on MacConkey agar with antibiotic selection. **(c)** M13 phage carrying pBluescript II can infect F+ *E. coli* in the gut. Mice were split into three experimental groups: (1) colonized with Sm^R W1655 F- and dosed with live M13(pBluescript II) (n = 3); (2) colonized with Sm^R W1655 F+ and dosed with heat-inactivated phage; (3) colonized with Sm^R W1655 F+ and dosed with live phage (n = 4). Colonized mice were treated with 10¹⁴ phage on Day 0 and carbencillin was added to the water. CFU per gram feces (black) and percent Carb^R (red) were determined on MacConkey agar with antibiotic selection. **(d)** M13-based delivery of antibiotic resistance gene is phage dose-dependent. M13(pBluescript II) was ten-fold serially diluted from 10¹⁴ to 10⁷. Mice (n = 24) were gavaged with a single dilution on Day 0 and carbencillin was added to the water. On Day 2, Carb^R CFU per gram feces was determined on MacConkey agar with antibiotic selection. Sm, streptomycin; Amp, ampicillin; Carb, carbencillin; dashed line, limit of detection for CFU per gram feces.

treatment (Figure 1b). When selection was lifted on Day 7, recolonization was observed for 5 of the 6 mice; when carbenicillin was again introduced on Day 13, colonization again dropped dramatically following dynamics similar to the first exposure. The very low background *E. coli* in the gut during carbenicillin treatment, as well as the lack of emergent spontaneous resistant cells able to recolonize during either the first or second antibiotic exposure, indicates that using a beta-lactam antibiotic in the drinking water is a very effective means of selection in our setup.

With an understanding of the dynamics of antibiotic selection *in vivo*, we next pursued the phage-mediated delivery of a resistance gene. Reports in the literature suggested that while M13 can withstand low pH [57], it may not fare so well in gastric juice [58]. We reasoned that we may be able to overcome this potential obstacle by relying on our selective power — that is, even if phage viability and frequency of infection events were low, the ability to apply selection for infected cells would give us an strong advantage for detection. To deliver a Carb^R gene to *E. coli* in the gut, we first generated M13 phage carrying pBluescript II using established methods for helper-mediated packaging of phagemid DNA. Next, we colonized mice with either Sm^R *E. coli* W1655 F+ (M13^S) or W1655 F- (M13^R as a control) and subsequently dosed them with either live phage or a heat-inactivated preparation of the same phage (Figure 1c). After dosing the mice with approximately 10¹⁴ M13 phage carrying Carb^R, we immediately transferred them to water containing carbenicillin, and then tracked both total *E. coli* and Carb^R *E. coli* in the feces for 7 days. Colonization levels fell rapidly and stayed near or below the limit of detection in control mice that were either colonized with F- and given live phage or colonized with F+ but given heat-inactivated phage; in contrast, when mice were colonized with F+ and dosed with live phage, there was only a transient drop in colonization on the first day, during which the rise of Carb^R cells occurred, and colonization was re-established within one day by an *E. coli* population that was resistant to carbenicillin (Figure 1c). These results show that orally dosed M13 phage were indeed able to

infect *E. coli* in the GI tract and deliver a plasmid conferring resistance to carbenicillin. 160

We confirmed these results in an independent animal experiment in which mice were colonized by 161
Sm^R *E. coli* W1655 F⁺ and orally dosed with ten-fold serial dilutions of phage carrying Carb^R, from 162
10¹⁴ phage down to 10⁷ phage (n = 2 or 3 per dose). We found that colonization by Carb^R *E. coli* 163
was consistent across high phage doses (10¹⁴ and 10¹³) but variable at lower doses (10¹² to 10⁹), 164
suggesting that factors other than number of phage introduced into the mouse can impact 165
colonization outcome (Figure 1d). We confirmed that resistance to carbenicillin was indeed due to 166
M13-mediated transfer of the plasmid pBluescript II by extracting plasmid DNA from fecal Carb^R 167
E. coli isolates from the 11 mice that were successfully colonized; comparison of 168
restriction-digested plasmid DNA to linearized pBluescript II confirmed that isolates from all 11 169
mice carried plasmid DNA of the expected size (Figure S3). These results show that plasmid DNA 170
was indeed transferred from M13 phage particles into recipient *E. coli* colonizing the GI tract. 171

M13 carrying CRISPR-Cas9 can target *E. coli* *in vitro* 172

We next asked whether M13 could be used to deliver vectors that carry CRISPR-Cas9 for 173
sequence-specific targeting of *E. coli*. We first generated two fluorescently marked isogenic 174
derivatives of Sm^R W1655 F⁺ using the *mcherry* or the *sfgfp* marker gene, with the goal of using 175
CRISPR-Cas9 to target the latter. We next constructed M13-compatible non-targeting (NT) and 176
GFP-targeting (GFPT) CRISPR-Cas9 vectors by cloning the spacers sequences, *bla* gene, and f1 177
origin of replication into the previously described low-copy vector pCas9 [59], generating 178
pCas9-NT-f1A/B and pCas9-GFPT-f1A/B (Figure S4). The *bla* and f1 *ori* were cloned as a fragment 179
from pBluescript II in both possible orientations (A or B) to make possible M13 ssDNA packaging of 180
either strand of vector DNA, a feature determined by the orientation of the f1 *ori*. We packaged 181
these phagemids into M13 using a helper strain and called resulting phage NT M13 or GFPT M13. 182
The phage were used to infect the GFP- or mCherry-marked strains and cells were diluted and 183

spotted on solid media containing carbenicillin to select for the transferred phagemid. We found 184
that GFP-marked *E. coli* infected with GFPT M13 exhibited impaired colony growth relative to the 185
NT M13 control (Figure 2a and Figure S5). Interestingly, we did not observe a large decrease in 186
the total number of CFUs indicating that despite impaired growth, M13-delivered CRISPR-Cas9 187
could be overcome by mechanisms enabling cell survival under targeting conditions. 188

Given that GFP-marked cells could withstand GFPT M13, we next focused on survivors to examine 189
possible means of escaping CRISPR-Cas9. We subjected colonies arising from infection with NT 190
M13 or GFPT M13 (Figure 2a) to streak purification and observed that of 16 clones from the GFPT 191
set, 11 lost GFP fluorescence while 5 maintained fluorescence (Figure 2b). We isolated genomic 192
DNA from these 16 clones, as well as 4 clones from the NT control, and used PCR to verify 193
presence or absence of the *sfgfp* gene. As expected, all 4 NT clones as well as the 5 GFPT clones 194
that retained GFP fluorescence possessed the *sfgfp* gene; analysis of the CRISPR-Cas9 195
phagemid revealed that of these latter 5 clones, 4 had lost the targeting spacer (Figure S6). In 196
contrast, the 11 non-fluorescent clones retained the spacer (Figure S6) and appeared to have 197
chromosomal deletions of or encompassing the target gene, with 10 being negative for a PCR 198
product (Figure 2c) and 1 exhibiting a partial loss of the coding sequence that includes the site 199
targeted by Cas9 under GFPT conditions (Figure S7). These data suggest that in most cases, 200
escape from CRISPR-Cas9 by target site mutation is accompanied by gene loss and are consistent 201
with previous work showing that chromosomal cleavage by Cas9 in *E. coli* can be repaired by 202
homologous recombination leading to large deletions up to 35 kb [60]. 203

Although it was possible for GFP-marked cells to overcome CRISPR-Cas9, we wanted to take 204
advantage of the growth defect of cells under targeting conditions; that is, because GFP-marked 205
E. coli showed impaired growth visible in colony morphology, we next asked if GFPT M13 infection 206
of a co-culture of GFP-marked and mCherry-marked strains would lead to the the former being 207

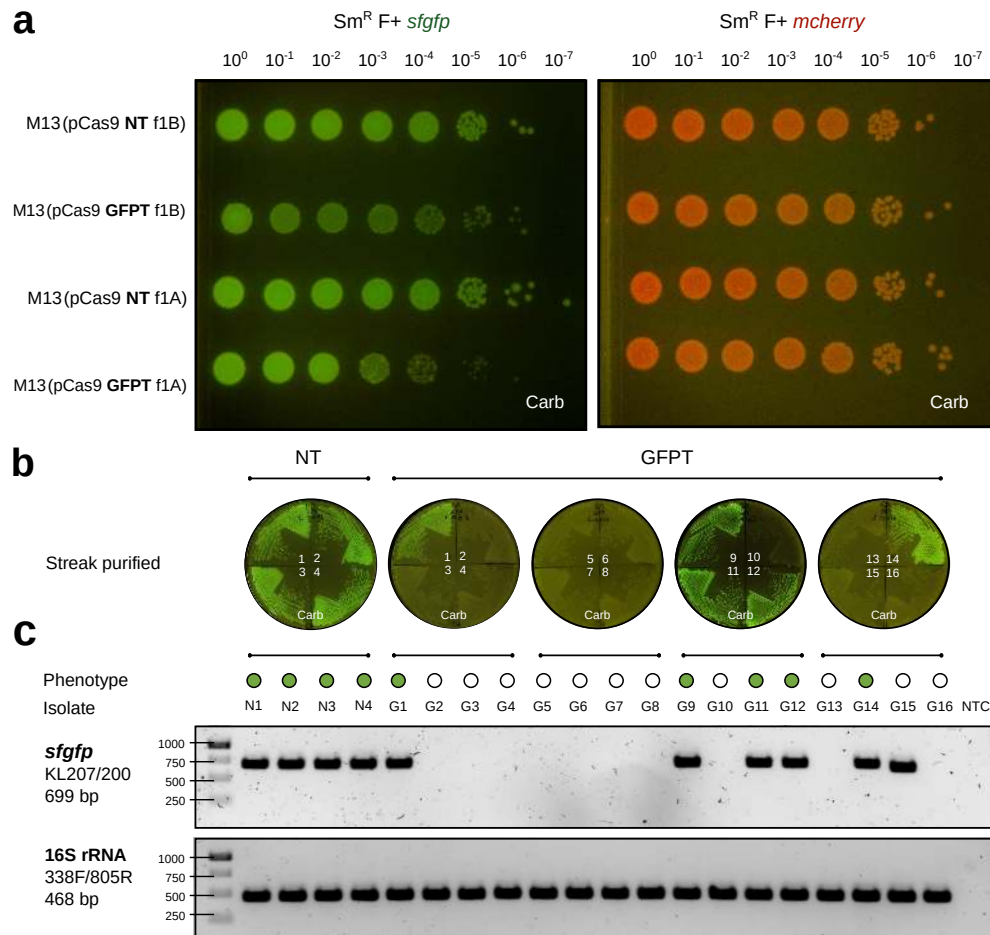


Figure 2. M13-mediated delivery of CRISPR-Cas9 to *E. coli* cells *in vitro* causes impaired colony growth and can induce chromosomal deletions that encompass the targeted gene. (a) GFP-marked *E. coli* exhibit a sick colony morphology after infection with M13 phage carrying GFP-targeting CRISPR-Cas9. M13 phage with non-targeting (NT) or GFP-targeting (GFPT) CRISPR-Cas9 were used to infect Sm^R F+ GFP-marked *E. coli* or mCherry-marked *E. coli* as a negative control. Cells were incubated with phage for infection then serially diluted and spotted onto media with selection for the CRISPR-Cas9 vector. Designation of f1A or f1B indicates the DNA strand of the vector in M13 phage, dependent on the orientation in which the f1-*bla* fragment was cloned. **(b)** CRISPR-Cas9 targeting the GFP gene can induce loss of fluorescence. Colonies arising from infection with M13 phage carrying either NT or GFPT CRISPR-Cas9 were subjected to several rounds of streak purification on selective media to ensure phenotypic homogeneity and clonality. The majority (11/16) of GFP-targeted streak purified clones lost GFP fluorescence. **(c)** Clones exhibiting a loss of fluorescence due to GFPT CRISPR-Cas9 have chromosomal deletions of or encompassing the targeted gene. Genomic DNA was isolated from streak-purified clones and PCR was used to determine whether the GFP gene was present; PCR for the 16S rRNA gene was performed as a positive control.

outcompeted. We started co-cultures of the two strains, adding either NT M13 or GFPT M13 208
followed by carbenicillin to select for phage infection of cells; we sampled the co-cultures every 4 h 209
over a period of 24 h by washing, diluting, and spotting cells onto non-selective solid media to 210
assess the relative abundance of the two strains. We found that GFPT M13 led to fewer 211
GFP-fluorescent colonies at 4 h and onwards, relative to the NT M13 control (Figure 3a). However, 212
we observed that at the later timepoints (16, 20, and 24 h), healthy GFP fluorescent colonies arose 213
at dilutions in which they were growth-impaired at earlier timepoints. We asked whether unimpaired 214
growth of the GFP-marked strain at these later timepoints could be due to enzymatic inactivation of 215
carbenicillin in the culture thereby relaxing the selection for the phagemid over time. We tested the 216
supernatant for carbenicillin using a bioassay with the indicator organism *Bacillus subtilis* 168 and 217
found that the vast majority of the antibiotic was not detected in cultures after 4 h whereas it was 218
detected at all timepoints in the sterile control (Figure 3b); furthermore, these GFP fluorescent 219
colonies were largely absent when the same co-culture was spotted onto media containing 220
carbenicillin (Figure S8), indicating that the recovery of GFP+ cells at later timepoints in the 221
co-culture could be due to lack of selection leading to loss of the phagemid carrying GFPT 222
CRISPR-Cas9. 223

To more quantitatively assess the abundance of the two fluorescent strains in competition after 224
infecting with NT or GFPT M13 phage, we turned to flow cytometry. We repeated the co-culturing 225
experiment in triplicate and quantified GFP+ and mCherry+ events 8 h after adding phage and 226
carbenicillin to select for phage infection. Compared to the NT control, the co-culture infected with 227
GFPT M13 exhibited both fewer GFP+ events (34% versus 62% for NT control; Figure 3c) as well 228
as a shift in the distribution of GFP+ events towards lower fluorescence leading to a bimodal 229
distribution (peak intensities of 44654 and 8943 versus a single peak of 31441 for the NT control; 230
Figure 3d). Interestingly, the relative abundance of GFP+ was higher than would be expected from 231

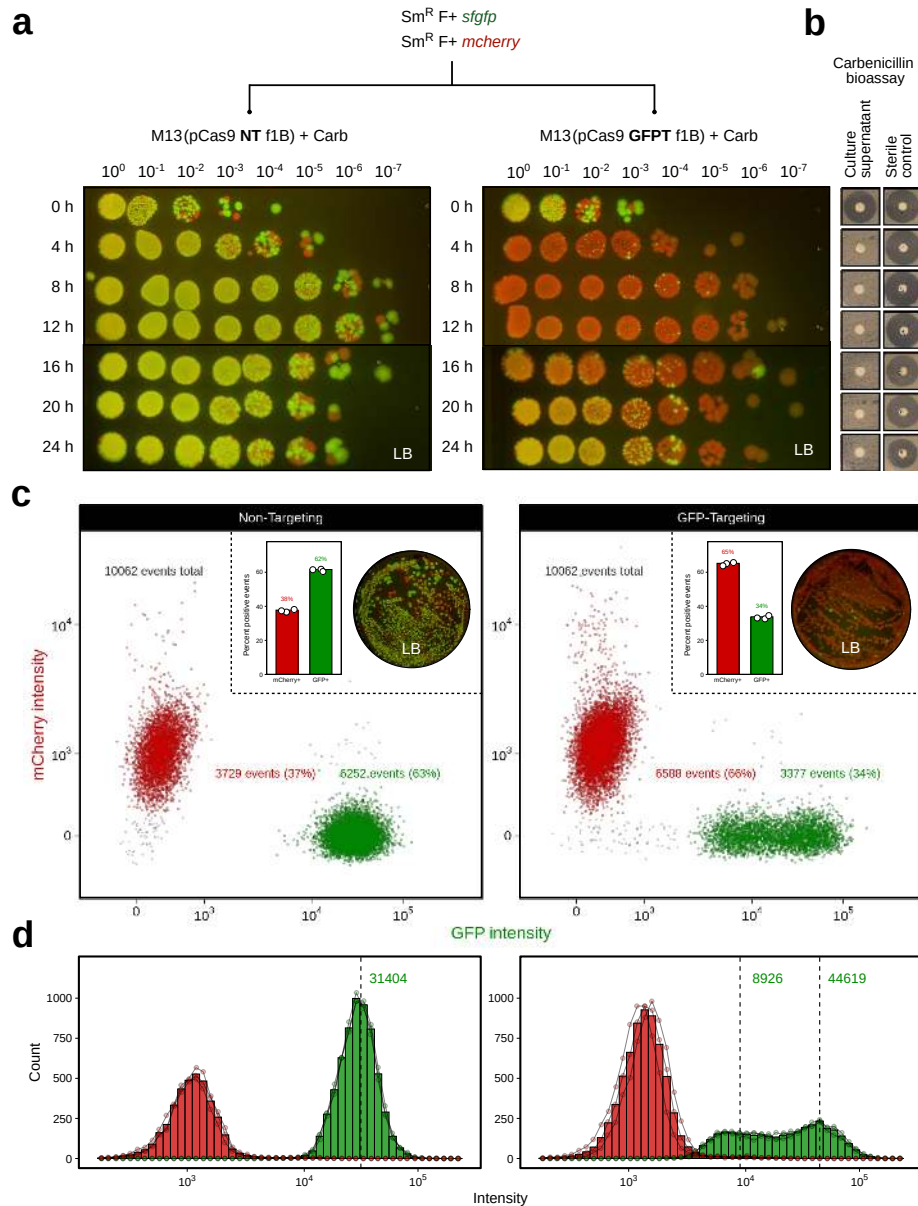


Figure 3. M13-delivered CRISPR-Cas9 for sequence-specific targeting of *E. coli* in *in vitro* co-cultures of fluorescently marked isogenic strains. (a) M13-delivered GFPT CRISPR-Cas9 leads to reduced competitive fitness of the GFP-marked strain. A co-culture of Sm^R F+ *sfGfp* and Sm^R F+ *mCherry* was incubated with M13 phage carrying non-targeting (NT) or GFP-targeting (GFPT) CRISPR-Cas9 at a starting MOI of approximately 500. Carbenicillin was added to a final concentration of 100 µg/µl to select for phage infection. Co-cultures were sampled every 4 hours over 24 hours; cells were washed, serially diluted, and spotted onto non-selective media to assess targeting of the GFP-marked strain. (b) Carbenicillin in culture supernatants was not detectable within 4 hours of growth, using a carbenicillin bioassay against indicator strain *Bacillus subtilis* 168; bioassay detection limit approximately 2.5 µg/µl. (c) Flow cytometry of co-cultures 8 hours following the addition of phage and carbenicillin show reduced GFP+ events in the GFPT versus NT condition. Flow plot shows data from one of three replicates. Inset: bar graph quantifying percent GFP+ and mCherry+ events for three replicates (left); plating results for a single replicate on non-selective media (right). (d) GFPT CRISPR-Cas9 changes the shape of the distribution of GFP+ population. Histogram of mCherry+ and GFP+ events by intensity shows that a proportion of GFP+ cells in the GFPT condition have shifted to a state of lower fluorescence. Bars indicate mean of three replicates; connected points are individual replicates.

plating results of the same co-cultures at 8 h (Figure 3c inset), indicating that GFP+ cells may be 232
able to survive in liquid media under targeting conditions but be unable to form colonies on solid 233
media. To confirm these results, we repeated flow cytometry on the co-cultures at 8 h and 24 h, 234
finding that GFP+ events further decreased at 24 h in the GFPT condition (17% versus 63% for NT; 235
Figure S9). Although there was a discrepancy between the flow cytometry and the plating results 236
likely due to differences in survival in liquid versus on solid media, both methods demonstrated that 237
M13 phage delivering GFP-targeting CRISPR-Cas9 can impair the GFP-marked strain. Given 238
these results *in vitro*, we next wanted to determine if GFPT M13 could be used to selectively target 239
E. coli in vivo. 240

Sequence-specific depletion of *E. coli in vivo* using M13-delivered CRISPR-Cas9 241

Because the mCherry-marked strain could outcompete the GFP-marked strain under targeting 242
conditions with GFPT M13, we next asked whether this was also true *in vivo*. To answer this 243
question, we returned to the streptomycin-treated mouse model. We introduced both Sm^R F+ *sfgfp* 244
and Sm^R F+ *mcherry* strains into mice, then orally dosed them with either 10¹¹ NT M13 or GFPT 245
M13 and added carbenicillin in the water to select for phage infection; after one week of 246
carbenicillin treatment, we removed it from the water and followed mice for an additional week to 247
determine whether phage-induced changes would persist in the absence of maintaining selection 248
(Figure 4a). We collected and assayed fecal samples using flow cytometry from 5 different 249
timepoints: Day -3, before introduction of fluorescent *E. coli* strains; Day 0, at which both strains 250
are present; Day 2, after phage and carbenicillin have been applied; Day 7, after one week of 251
carbenicillin treatment; and Day 14, one week after carbenicillin was removed (Figure 4b shows 252
example time series flow cytometry data for one mouse from each of the NT and GFPT group; all 253
data are shown in Figure S10). 254

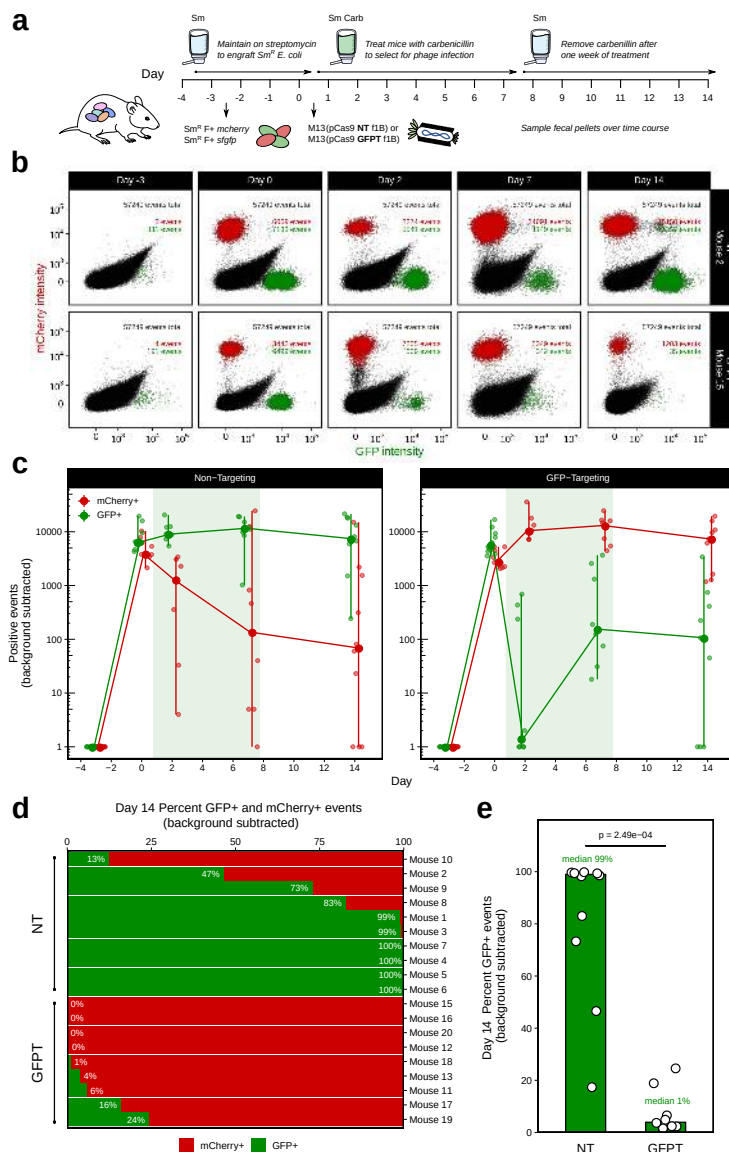


Figure 4. M13-delivered CRISPR-Cas9 for sequence-specific depletion of *E. coli* in the gut of mice colonized by competing fluorescently marked isogenic strains. (a) Experimental timeline: Day -3, mice were colonized with an approximately 50/50 mixture of *Sm^R F+ *stgfp** and *mCherry* using the streptomycin treatment model; Day 0, mice were dosed with 10^{11} M13 phage carrying non-targeting (NT) or GFP-targeting (GFPT) CRISPR-Cas9 (n = 10 per group) and carbenicillin was added to the drinking water; Day 7, carbenicillin was removed from the drinking water; Day 14, experimental endpoint. Fecal samples were collected throughout for analysis. (b) M13-delivered GFPT CRISPR-Cas9 can lead to loss of the GFP-marked strain. Time series flow plots of fecal samples for select mice, one from each of the NT and GFPT groups. Top right: total number of events as well as number of red and green events. (c) Mice in the GFP-targeting group exhibited a decrease in the number of GFP+ events in fecal samples over time compared to the non-targeting control group. For each mouse, GFP+ and mCherry+ events from Day -3 (before introduction of *E. coli*) were used to subtract background at all subsequent timepoints; timepoints were excluded in which both the GFP+ and the mCherry+ events were below a background threshold of maximum background observed for that fluorophore multiplied by a factor of three. Line graph: points indicate median; vertical lines indicate range of values observed. (d) Mice in the GFPT group exhibited depletion and even loss of the GFP-marked strain. Percent GFP+ and mCherry+ events for each mouse on Day 14. Mice were excluded if both the GFP+ and mCherry+ events were both below their respective background thresholds. (e) A significant difference was observed in the distribution of mice in the GFPT group versus NT control with respect to GFP+ events in fecal samples at Day 14. Bars are medians; p-value, Mann-Whitney test. Sm, streptomycin; Carb, carbenicillin.

For each mouse, we tracked GFP+ and mCherry+ events, using data from Day -3 (prior to *E. coli*) 255
to subtract background positive events for both fluorophores, on a per mouse basis. We found that 256
on average, while the GFP-marked strain appeared to fair better *in vivo* than the mCherry strain 257
under NT conditions, GFP+ events under GFPT conditions exhibited a sharp decrease on Day 2, 258
with some mice exhibiting levels at or near background; this was followed by a slight recovery on 259
Days 7 and 14 but to levels markedly below those in the NT control (Figure 4c; individual mouse 260
data are shown in Figure S11). We confirmed the large decrease in GFP+ events on Day 2 by 261
culturing from mouse fecal samples, finding that culturing results were consistent with flow 262
cytometry data (Figure S12). 263

At the final timepoint, 14 days after receiving phage, the relative abundance of GFP+ events in the 264
fecal samples of mice in the GFPT group was significantly different than the NT group ($p = 2.5e-4$, 265
Mann-Whitney test); furthermore, in 4 mice that received GFPT M13, the GFP-marked strain was 266
successfully outcompeted by the mCherry strain and GFP+ events were not detected above 267
background levels, an outcome that was not observed for any mouse in the NT condition (Figure 4d 268
and e). In fact, for mice receiving NT M13, the opposite tended to be true: we observed that the 269
relative abundance of GFP+ events was much higher on average than mCherry+ events (median 270
99% GFP+ for NT). These *in vivo* competition data indicate that it is possible to use M13 phage 271
carrying CRISPR-Cas9 for sequence-specific depletion of an otherwise isogenic bacterial strain in 272
the mouse gut. 273

M13-delivered CRISPR-Cas9 can induce chromosomal deletions *in vivo* 274

With positive results for strain-specific targeting using CRISPR-Cas9 against one of two strains 275
both *in vitro* and *in vivo*, we next returned to the idea of using GFPT M13 against only a single 276
strain of *E. coli* in the gut. That is, would it be possible to select for cells that have escaped 277
CRISPR-Cas9 targeting through genomic deletion events *in vivo*, as was observed *in vitro* 278

(Figure 2c)? To answer this question, we first constructed a double-marked Sm^R F+ *sfgfp mcherry* strain so that we could use flow cytometry to visualize loss of GFP fluorescence in mouse fecal samples, reasoning that double-positive events would shift to singly mCherry-positive events if the targeted *sfgfp* gene were to be lost. Following a similar regimen as the *in vivo* competition experiment (Figure 4a), we introduced the double-marked GFP+ mCherry+ strain into mice, then orally dosed them with either 10¹¹ NT M13 or GFPT M13 and added carbenicillin in the water; after one week, we removed carbenicillin and followed mice for another week (Figure 5a).

Again, we collected and assayed fecal samples using flow cytometry from 5 different timepoints: Day -5, before introduction of fluorescent *E. coli*; Day 0, when the strain is present; Day 2, after phage and carbenicillin have been applied; Day 7, after one week of carbenicillin treatment; and Day 14, one week after carbenicillin was removed. For each mouse, we used fluorescence levels on Day -5 (pre-*E. coli*) to account for background GFP+ mCherry+ events and those on Day 0 (pre-phage) to account for background mCherry+ events. After phage treatment, we observed the emergence of singly positive mCherry+ events in a subset of the mice given GFPT M13, an outcome that was not observed for the NT control, indicating cells had lost GFP fluorescence *in vivo* (Figure 5b shows example time series flow cytometry data for one mouse from each of the NT and GFPT group; all data are shown in Figure S13).

We tracked fluorescent events over time (Figure S14a) and found that by the final timepoint, mCherry+ events were detected in the fecal samples of 3 of 8 mice that remained positive for either singly or doubly positive events over background, with the relative abundance of the mCherry+ population being highly variable at 12%, 49%, and 96% (Figure 5c). We confirmed these outcomes by culturing from GFPT mouse fecal samples on Day 14, finding presence of red fluorescent colonies in proportions consistent with flow cytometry results (Figure 5d and Figure S14b). These data indicate that while it is possible for CRISPR-Cas9-induced genomic deletion events to occur *in*

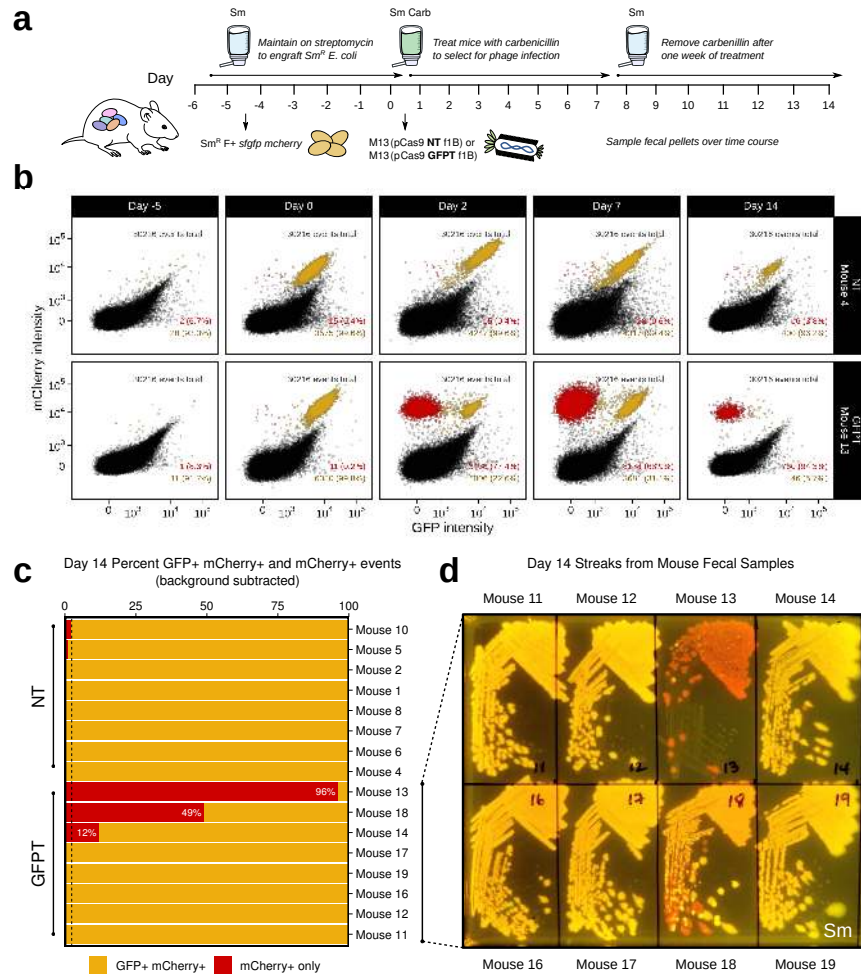


Figure 5. M13-delivered CRISPR-Cas9 can induce chromosomal deletions encompassing the targeted gene in *E. coli* colonizing the mouse gut. (a) Experimental timeline: Day -5, mice were colonized with double-marked *Sm^R F+ sfGFP mCherry* using the streptomycin treatment model; Day 0, mice were dosed with 10^{11} M13 phage carrying non-targeting (NT) or GFP-targeting (GFPT) CRISPR-Cas9 ($n = 10$ per group) and carbenicillin was added to the drinking water; Day 7, carbenicillin was removed from the drinking water; Day 14, experimental endpoint. Fecal samples were collected throughout for analysis. (b) M13-delivered GFPT CRISPR-Cas9 can cause loss of GFP fluorescence in double-marked *E. coli*. Time series flow plots of fecal samples for select mice, one from each of the NT and GFPT groups. Top right: total number of events; bottom right: singly mCherry+ events and doubly GFP+ mCherry+ events. (c) Fecal samples of three of eight mice in the GFPT group were positive for mCherry-only fluorescence on Day 14. Percent GFP+ mCherry+ and mCherry+ only events for each mouse. Mice were excluded if both populations were below a background threshold of maximum background observed for that population multiplied by a factor of three. Dashed line indicates maximum mCherry fluorescence observed for the NT group. (d) Culture of *E. coli* from fecal samples of the GFPT group on Day 14 confirmed loss of GFP leading to red rather than dual fluorescence. Colonies exhibiting only red fluorescence were observed for Mouse 13, 14, and 18 in proportions consistent with flow cytometry results. Sm, streptomycin; Carb, carbenicillin.

vivo, resultant deletion strains may or may not outcompete the parent strain. Furthermore, 5 of 8 mice in the GFPT group remained colonized by only the double-marked strain, suggesting that escape from CRISPR-Cas9 targeting through chromosomal deletion events may be a more improbable outcome than escape via mutations that inactivate the CRISPR-Cas9 system. Because spacer loss via plasmid recombination is a common mode of escape, we isolated singly (red) and doubly (yellow) fluorescent *E. coli* from feces of mice on Day 2 and extracted plasmid DNA to ask whether phagemids still carried the expected spacer. All fluorescent yellow isolates from NT mice had the expected spacer, as well as all fluorescent red isolates from GFPT mice; however, phagemid DNA isolated from fluorescent yellow isolates from the GFPT mice had all undergone recombination events, with 4 of 5 confirmed to have recombined only within the CRISPR array leading to loss of the spacer targeting the *sfgfp* gene (Figure S15).

Discussion

In this work, we use phage M13 and its host *E. coli* to demonstrate that bacterial viruses can be used for gene delivery to bacterial cells that are colonizing the gut. Specifically, in a series of highly controlled experiments using a standard phagemid vector, we show that M13 can infect and transfer the vector to *E. coli* engrafted in the gut of mice. We then construct phagemid vectors carrying CRISPR-Cas9 and use M13 as chassis to deliver these constructs to *E. coli*. Using strain competition in the gut, we first show that CRISPR-Cas9 targeting is sequence-specific and able to selectively decrease the abundance of the targeted strain. Second, in the absence of competition with a non-targeted strain, we show that M13-delivered CRISPR-Cas9 can generate loss of the target gene *in vivo* through homologous recombination, indicating that CRISPR-Cas9 can be employed to remove genes from bacteria while still enabling cell survival.

Development of CRISPR-Cas9 to target bacteria in the gut requires careful consideration of the mechanisms by which cells may escape killing. Although the use of M13-delivered CRISPR-Cas9 as an antimicrobial has been proposed [23], bacterial cells have been shown to be able to survive Cas9-induced double-stranded breaks by homologous recombination or non-homologous end-joining mechanisms [60]. In particular, RecA-mediated homology-directed repair is a highly conserved and robust response wherein induced cells may find a repair template sharing homology within minutes [61]. That targeted strains can readily escape killing suggests that rather than being used as an antimicrobial in the gut, phage-delivered CRISPR-Cas9 may instead be well suited for gut microbiome editing in the form of targeted genomic deletions, leveraging the conserved DNA repair pathways present in bacteria. One advantage of this approach is that specific genes could be targeted for removal from the gut microbiome whilst the community as a whole remains more intact than if the organism were to be removed entirely. This idea is consistent with previous use of CRISPR-Cas9 to target plasmid rather than chromosomal DNA [23, 24, 62]. An alternative to Cas9 would be to use CRISPR-Cas3 systems in which the larger DNA lesions may be more difficult to repair [63], although spacer loss leading to escape by *C. difficile* in the mouse gut has also been reported [26]. Likely irrespective of the particular system chosen for deployment *in vivo*, gut microbiome editing will require iterative improvements on the design of delivered CRISPR-Cas constructs to try to mitigate mutations that render the system inactive, or to decrease the probability of these events relative to either killing or gene loss events, the probability of which may also be locus-dependent.

Here, we demonstrate that filamentous phage can be used to deliver genetic cargo to bacterial cells in the mouse gut using CRISPR-Cas9 as proof-of-concept, but there are many potential applications for gene delivery to commensal bacteria. Furthermore, although we use phage in combination with an antibiotic treatment, alternative (i.e., non-antibiotic) strategies to select for or

enrich for cells that have been infected in the gut would be immensely useful to minimize large 349
disruptions to the existing gut microbiota. Issues including phage survival, phage infection 350
frequency, and selection for cells that have been infected by phage may be influenced by the 351
choice of phage chassis, target bacterium, and cargo design. These factors will have to be well 352
understood if the potential of phage-based gene delivery to the microbiota is to be fully realized. 353
Foundational, reductionist, and highly controlled studies such as ours will be valuable not only to 354
establish *in vivo* models with which to study specific phage-bacteria interactions but also to assess 355
the feasibility, utility, and possible limitations of phage-based gene delivery, particularly as the 356
microbiome research community aspires to the genetic manipulation of diverse bacterial members 357
of the gut microbiota and turns to phage as potential tools for *in vivo* microbiome editing. 358

Acknowledgments

359

We thank Jessie Turnbaugh, Kimberly Ly, Jolie Ma, and staff at the UCSF animal facility for animal 360
care and assistance with learning animal procedures. We are grateful to Daryll Gempis, Bernarda 361
Lopez, and Ernesto Valencia of the UCSF G.W. Hooper Foundation for laboratory and 362
administrative support. We thank Katja Engel (University of Waterloo) for help in translating the 363
original publication on the isolation of M13 written in German. We are grateful to Antoine Vigouroux 364
(Institut Pasteur) for generously sharing MG1655 derivatives carrying *sfgfp* and *mcherry* marker 365
genes. We thank the Chan-Zuckerberg BioHub for sequencing through the Microbiome Initiative. 366
We are grateful to Joseph Bondy-Denomy and Oren Rosenberg (UCSF) for constructive criticism 367
on the manuscript. The graphic of a laboratory mouse was adapted from a Wikimedia Commons 368
graphic distributed under CC-BY-SA-4.0 by Gwilz. 369

Author Contributions

370

KNL and PJT conceived the ideas. KNL supervised laboratory work and analyzed the data. KNL, 371
PS, PSP, and PJT designed the experiments. KNL and PS constructed *E. coli* strains. KNL and 372
PSP constructed plasmids. KNL performed phage and animal experiments with assistance from 373
PSP. PS and KNL performed antibiotic assays. KNL, FBY, and JEB performed 16S rRNA gene 374
sequencing with assistance from PSP and MN. MA performed flow cytometry with assistance from 375
KNL. KNL analyzed mouse fecal isolates with assistance from MN. PJT provided reagents and 376
materials. KNL made the figures and drafted the manuscript; PJT, PS, PSP, MA, JEB, and FBY 377
assisted with editing. 378

Funding

379

KNL and PS were both supported by a postdoctoral fellowship from the Canadian Institutes of Health Research (CIHR), JEB by a postdoctoral fellowship from the Natural Sciences and Engineering Research Council of Canada (NSERC), MA by an F32 fellowship from the National Institutes of Health (F32AI147456-01), and PSP by a scholarship from the UCSF Discovery Fellows Program. This work was supported by the National Institutes of Health (PJT, R01HL122593). PJT holds an Investigators in the Pathogenesis of Infectious Disease Award from the Burroughs Wellcome Fund, is a Chan Zuckerberg Biohub investigator, and was a Nadia's Gift Foundation Innovator supported, in part, by the Damon Runyon Cancer Research Foundation (DRR-42-16) and the Searle Scholars Program (SSP-2016-1352).

Conflict of Interest Statement

389

KNL, PS, and PJT are listed inventors on a U.S. provisional patent application related to this work (33167/55262P1). PJT is on the scientific advisory boards for Kaleido, Pendulum, Seres, and SNIPRbiome. All other authors declare no competing interests.

Methods

393

Bacterial strains, plasmids, phage, and oligonucleotides. Strains, plasmids, and phage used

394

in this study, including description and sources, are provided in [Table 1](#). Oligonucleotides used in

395

this study are provided in [Table 2](#).

396

Table 1. Bacterial strains, plasmids, and phage.

Resource	Relevant Characteristics	Ref./Source
Strain		
XL1-Blue MRF ⁺	Phage propagation with helper M13KO7; Tc ^R	Agilent
DH5alpha	Routine cloning; phage propagation with helper HP4_M13	[64]
MG1655	Derivative of K-12	[65]
W1655 F ⁻	Derivative of K-12; M13 ^R	ATCC 23737
W1655 F ⁺	Derivative of K-12; M13 ^S	ATCC 23590
MG1655 <i>rpsL</i> -Sm ^R	Spontaneous <i>rpsL</i> -Sm ^R (Lys42Arg) derivative of MG1655	This study
W1655 F ⁻ <i>rpsL</i> -Sm ^R	Recombineered <i>rpsL</i> -Sm ^R (Lys42Arg) derivative of W1655 F ⁻	This study
W1655 F ⁺ <i>rpsL</i> -Sm ^R	Recombineered <i>rpsL</i> -Sm ^R (Lys42Arg) derivative of W1655 F ⁺	This study
AV01::pAV01	MG1655 with constitutive <i>sfgfp</i> clonetedegrated at HK022 <i>att</i> site; Km ^R	[66]
AV01::pAV02	MG1655 with constitutive <i>mcherry</i> clonetedegrated at lambda <i>att</i> site; Km ^R	[66]
W1655 F ⁺ <i>rpsL</i> -Sm ^R <i>sfgfp</i>	Sm ^R W1655 F ⁺ with <i>sfgfp</i> transduced from AV01::pAV01; Km ^S	This study
W1655 F ⁺ <i>rpsL</i> -Sm ^R <i>mcherry</i>	Sm ^R W1655 F ⁺ with <i>mcherry</i> transduced from AV01::pAV02; Km ^S	This study
W1655 F ⁺ <i>rpsL</i> -Sm ^R <i>sfgfp mcherry</i>	Sm ^R W1655 F ⁺ <i>sfgfp</i> with <i>mcherry</i> transduced from AV01::pAV02; Km ^S	This study
Plasmid		
pBluescript II KS(-)	Commercial phagemid; Carb ^R	Agilent
pSIJ8	Temperature-sensitive; lambda Red recombineering; Carb ^R	[67]
pE-FLP	Temperature sensitive; constitutive flippase expression; Carb ^R	[68]
pCas9	Low-copy vector carrying <i>cas9</i> , <i>tracrRNA</i> , and CRISPR array; Cm ^R	[59]
pCas9-NT-f1A	pCas9 with non-targeting spacer; f1- <i>bla</i> in orientation A; Cm ^R Carb ^R	This study
pCas9-NT-f1B	pCas9 with non-targeting spacer; f1- <i>bla</i> in orientation B; Cm ^R Carb ^R	This study
pCas9-GFPT-f1A	pCas9 with GFP-targeting spacer; f1- <i>bla</i> in orientation A; Cm ^R Carb ^R	This study
pCas9-GFPT-f1B	pCas9 with GFP-targeting spacer; f1- <i>bla</i> in orientation B; Cm ^R Carb ^R	This study
Phage / Helper		
M13KO7	Helper phage; Km ^R	NEB
HP4_M13	Helper plasmid; Km ^R	[69]
P1	Transducing phage	ATCC 25404-B1

Table 2. Oligonucleotides used in this study.

Oligo ID	Oligo Sequence 5'–3'	Purpose
PS-rpsL1	CGTGGCATGGAATACTCCG	F primer to amplify <i>rpsL</i> for recombineering
PS-rpsL2	GCATCGCCCTAAAATTCGGC	R primer to amplify <i>rpsL</i> for recombineering
PSP116	AAACCCCTTACCTTCACCACGAACAGAAATTTG	Oligo 1 to generate GFPT spacer
PSP117	AAAACAAATCTCTGTTCGTGGTGAAGTGAAGG	Oligo 2 to generate GFPT spacer
PSP120	AAACATCGCACATCCTGGTCGCGACATTAAGAGT	Oligo 1 to generate NT spacer
PSP121	AAAAACTCTTAATGTGCGGACCAGGATGTGCGAT	Oligo 2 to generate NT spacer
PSP108	TTAATAAATGCAGTAATACAGG	Primer to sequence spacer in CRISPR array
KL215	CCTGTCGACGGTATCGATAAGCTTGATATCG	F primer to clone <i>f1-bla</i> from pBluescript II as Sall fragment
KL216	CCTGTCGACGATTATCAAAAAGGATCTTACCTAGATCC	R primer to clone <i>f1-bla</i> from pBluescript II as Sall fragment
KL207	CTGTTACCGGTGTTGTTCC	F primer to amplify <i>stgfp</i> fragment
KL200	TTATTTGTAGAGTTTCATCCATGCCG	R primer to amplify <i>stgfp</i> fragment
BAC338F	ACTCCTACGGGAGGCAG	F primer to amplify 16S rRNA gene fragment
BAC805R	GACTACCGGGTATCTAATCC	R primer to amplify 16S rRNA gene fragment
V4 515F Nextera	TCGTCGGCAGCGTCAGATGTGTATAAGAGACAGGTGCCA GCMGCCGCGGTAA	F primer for 16S rRNA gene sequencing primary PCR
V4 806R Nextera	GTCTCGTGGGCTCGGAGATGTGTATAAGAGACAGGGACT ACHVGGGTWTCTAAT	R primer for 16S rRNA gene sequencing primary PCR
Various (Table S1)	AATGATACGGCGACCACCGAGATCTACACNNNNNNNTC GTCGGCAGCGTC	F primer for 16S rRNA gene sequencing indexing PCR
Various (Table S1)	CAAGCAGAAGACGGCATACGAGATNNNNNNNGTCTCGT GGGCTCGG	R primer for 16S rRNA gene sequencing indexing PCR

Minimum inhibitory concentration (MIC) assay. Cells were prepared by standardizing an 397
overnight culture to an OD₆₀₀ of 0.1 using saline, and further diluted ten-fold in saline then ten-fold 398
in LB. The drug was prepared by dissolving antibiotic in vehicle (sterile distilled water) and 399
filter-sterilizing, then serially diluting two-fold in vehicle to prepare 100× stock solutions, and finally 400
diluting ten-fold in LB for 10× stock. To wells of a 96-well plate, 60 μl of LB, 15 μl of drug, and 75 μl 401
of cells were added and mixed well. Final drug concentrations ranged between 0.002 μg/ml to 402
1000 μg/ml for ampicillin and 0.24 μg/ml to 2000 μg/ml for carbenicillin. The plate was incubated 403
overnight at 37 °C without shaking and OD₆₀₀ was measured the following morning after agitation. 404

16S rRNA gene sequencing. Mouse fecal pellets were stored at –80 °C, DNA was extracted from 405
single pellets using a ZymoBIOMICS 96 MagBead DNA Kit, and 16S rRNA gene sequencing was 406
performed using a dual indexing strategy [70]. Briefly, primary PCR was performed using KAPA 407

HiFi Hot Start DNA polymerase (KAPA KK2502) and V4 515F/806R Nextera primers (Table 1). The reaction was diluted in UltraPure DNase/RNase-free water (Life Tech 0977-023) and used as template for a secondary (indexing) PCR using sample-specific dual indexing primers (Table 2 and Table S1). The reactions were normalized using a SequelPrep Normalization plate (Life Tech A10510-01) and the DNA was eluted and pooled. To purify and concentrate the DNA, 5 volumes of PB Buffer (Qiagen 28004) was added, mixed thoroughly, and purified using a QIAquick PCR Purification Kit (Qiagen 28106). The DNA was gel extracted using a MinElute Gel Extraction Kit (Qiagen 28604), quantified by qPCR using a KAPA Library Quantification Kit for Illumina Platforms (KAPA KK4824), and paired-end sequenced on the Illumina MiSeq platform. Data were processed using a 16S rRNA gene analysis pipeline [71] based on QIIME2 [72] incorporating DADA2 [73], and analyzed using R packages *qiime2R* v0.99.23 [74], *phyloseq* v1.33.0 [75], and *phylosmith* v1.0.4 [76]. Sample metadata are provided (Table S2) and raw sequence data have been deposited at the NCBI Sequence Read Archive under BioProject PRJNA642411 with accession numbers 12118792 to 12118959.

Construction of streptomycin-resistant *E. coli* strains. Strains resistant to the antibiotic streptomycin were generated by either selection for spontaneous resistance or by lambda Red recombineering [67, 77]. Spontaneous resistant mutants were selected by plating overnight cultures on LB supplemented with 500 µg/ml streptomycin. Lambda Red recombineering was later used to introduce a specific allele for genetic consistency between strains as different mutations in the *rpsL* gene can confer resistance to streptomycin [78]. Briefly, cells were transformed with the Carb^R temperature-sensitive plasmid pSIJ8 [67], and electrocompetent cells were prepared from cells grown in LB carbenicillin at 30 °C to early exponential phase and lambda Red recombinase genes were induced by addition of L-arabinose to 7.5 mM. Cells were electroporated with an *rpsL*-Sm^R PCR product amplified from a spontaneous streptomycin-resistant mutant of MG1655

using primers PS-rpsL1 and PS-rpsL2, and recombinants were selected on LB supplemented with 432
500 µg/ml streptomycin. The pSIJ8 plasmid was cured by culturing in liquid at 37 °C in the absence 433
of carbencillin, plating for single colonies, and confirming Carb^S. The *rpsL* gene of Sm^R strains 434
were confirmed by Sanger sequencing ([Figure S16](#)). 435

Construction of fluorescently marked *E. coli* strains. P1 lysates were generated of 436
AV01::pAV01 and AV01::pAV02 carrying clonotegrated *sfgfp* and *mcherry*, respectively [66]. Briefly, 437
150 µl of overnight culture in LB supplemented with 12.5 µg/ml kanamycin was mixed with 1 µl to 438
25 µl P1 phage (initially propagated from ATCC on MG1655). The mixture was incubated for 10 439
minutes at 30 °C to aid adsorption, added to 4 ml LB 0.7% agar, and overlaid on pre-warmed LB 440
agar supplemented with 25 µg/ml kanamycin 10 mM MgSO₄. Plates were incubated overnight at 441
30 °C, and phage were harvested by adding 5 ml SM buffer, incubating at room temperature for 10 442
minutes, and breaking and scraping off the top agar into a conical tube. Phage suspensions were 443
centrifuged to pellet agar; the supernatant was passed through a 100 µm cell strainer, then through 444
a 0.45 µm syringe filter, and lysates were stored at 4 °C. For transduction, 1-2 ml of recipient 445
overnight culture was pelleted and resuspended in 1/3 volume LB 10 mM MgSO₄ 5 mM CaCl₂. 446
100 µl of cells was mixed with 1 µl to 10 µl P1 lysate and incubated at 30 °C for 60 minutes. To 447
minimize secondary infections, 200 µl 1 M sodium citrate was added, followed by 1 ml of LB. The 448
mixture was incubated at 30 °C for 2 h, then plated on LB 10 mM sodium citrate 25 µg/ml 449
kanamycin to select for transductants. For excision of the vector backbone including the kanamycin 450
resistance gene and heat-inducible integrase, cells were electroporated with pE-FLP [68]; 451
transformants were selected on carbencillin and confirmed for Km^S. pE-FLP was cured by 452
culturing in liquid at 37 °C in the absence of carbencillin, plating for single colonies, and confirming 453
Carb^S. Strains were subsequently grown routinely at 37 °C. For imaging fluorescent strains on 454
agar, plates were typically incubated at 37 °C overnight, transferred to room temperature to allow 455

fluorescence intensity to increase, and then imaged. 456

Engrafting *E. coli* in mice and preparation of antibiotic drinking water. Animal procedures 457
were approved by the UCSF Institutional Animal Care and Use Committee. Specific pathogen free 458
female BALB/c mice from the vendor Taconic were used for all mouse experiments. Streptomycin 459
water was prepared by dissolving USP grade streptomycin sulfate (VWR 0382) in autoclaved tap 460
water to a final concentration of 5 mg/ml and passing through 0.45 µm filtration units. Mice were 461
provided streptomycin water for 1 day, followed by oral gavage of 0.2 ml containing approximately 462
10⁹ CFU streptomycin-resistant *E. coli*. Mice were kept on streptomycin water thereafter to 463
maintain colonization. For selection with beta-lactam antibiotics, USP grade ampicillin sodium salt 464
(Teknova A9510) or USP grade carbenicillin disodium salt (Teknova C2110) was also dissolved in 465
the water to a final concentration of 1 mg/ml. Drinking water containing streptomycin was prepared 466
fresh weekly; with the addition of a beta lactam antibiotic, it was prepared fresh every 3-4 days. 467

Enumeration and culture of *E. coli* from mouse feces. Fecal pellets were collected from 468
individual mice and CFU counts were performed on the same day. CFU per gram of feces was 469
estimated by weighing the fecal pellet (typically 10-40 mg) on an analytical balance and suspending 470
in 250 µl to 500 µl PBS or saline by manual mixing and vigorous vortexing. Large particulate matter 471
was pelleted by centrifuging at 100×g, ten-fold serial dilutions were made in PBS, and 5 µl of each 472
dilution was spotted on Difco MacConkey agar (BD 212123) supplemented with the appropriate 473
antibiotics, i.e., streptomycin (100 µg/ml) or carbenicillin (50 µg/ml). For qualitative assessment of 474
the fluorescent strains in feces, samples were spotted onto LB supplemented with the appropriate 475
antibiotics. For isolating *E. coli* from fecal samples for genomic or plasmid DNA analysis, 10 µl to 476
50 µl of the fecal suspension was streaked on agar, and single colonies were further streak-purified. 477

Construction of CRISPR-Cas9 phagemid vectors. Cultures were grown in LB or TB media 478
supplemented with the appropriate antibiotics. Plasmid DNA was prepared by QIAprep Spin 479

Miniprep Kit (Qiagen 27106), eluted in TE buffer, and incubated at 60 °C for 10 minutes. Samples 480
were quantified using a NanoDrop One spectrophotometer. The vector pCas9 [59] was digested 481
with Bsal (NEB R0535) and gel extracted with a QIAquick Gel Extraction Kit (Qiagen 28706). 482
Spacers were generated by annealing and phosphorylating the two oligos (PSP116 and PSP117 483
for GFPT; PSP120 and PSP121 for NT [66]) at 10 μM each in T4 ligation buffer (NEB B0202S) with 484
T4 polynucleotide kinase (NEB M0201S) by incubating at 37 °C for 2 hours, 95 °C for 5 minutes, 485
and ramping down to 20 °C at 5 °C/min. The annealed product was diluted 1 in 200 in sterile 486
distilled water and used for directional cloning by ligating (Thermo Scientific FEREL0011) to 60 ng 487
of Bsal-digested, gel extracted pCas9 overnight at room temperature. Ligations were used to 488
transform 5-alpha competent cells (NEB C2987H) and the cloned spacer was verified by Sanger 489
sequencing using primer PSP108. The trailing repeat was later confirmed to lack the starting 5'G, 490
which did not interfere with GFP-targeting function. The 1.8-kb fragment carrying the f1 origin of 491
replication and beta-lactamase gene (*f1-bla*) was amplified from pBluescript II with Sall adapters 492
using primers KL215 and KL216 and KOD Hot Start DNA polymerase (Millipore 71842-3). The 493
PCR product was purified using a QIAquick PCR Purification Kit (Qiagen 28104), digested with Sall 494
(Thermo Fisher FD0644), gel extracted, and used to ligate to Sall-digested, 495
FastAP-dephosphorylated (Thermo Fisher FEREF0651) vector. Ligations were used to transform 496
DH5alpha and clones were screened by restriction digest for both possible insert orientations (A or 497
B) using Xbal (Thermo Scientific FD0684) and one of each orientation was saved for both the 498
GFPT and NT phagemids. 499

Preparation of M13 carrying pBluescript II. This protocol was adapted from those to generate 500
phage display libraries [79]. XL1-Blue MRF' was transformed with pBluescript II (Agilent 212208). 501
An overnight culture of this strain was prepared in 5 ml LB supplemented with tetracycline (5 μg/ml) 502
and carbenicillin (50 μg/ml) and subcultured the following day 1-in-100 into 5 ml 2YT supplemented 503

with the same antibiotics. At an OD₆₀₀ of 0.8, cells were infected with helper phage M13KO7 (NEB 504 N0315S) at a multiplicity of infection of approximately 10:1 for 1 h at 37 °C. The infected cells were 505 used to seed 2YT supplemented with carbenicillin (100 µg/ml) and kanamycin (25 µg/ml) at 506 1-in-100, and the culture was grown overnight to produce phage. Cells were pelleted at 10,000×g 507 for 15 minutes, and the supernatant containing phage was transferred. Phage were precipitated by 508 adding 0.2 volumes phage precipitation solution (20% PEG-8000, 2.5 M NaCl), inverting to mix 509 well, and incubating for 30 minutes on ice. Phage were pelleted at 15,000×g for 15 minutes at 4 °C 510 and the supernatant was discarded. The phage pellet was resuspended in PBS at 1-4% of the 511 culture volume. The resuspension was centrifuged to pellet insoluble material and transferred to a 512 new tube. Glycerol was added to a final concentration of 10-15%. Phage preparations were 513 aliquoted into cryovials and frozen at –80 °C for long-term storage. 514

Preparation of M13 carrying CRISPR-Cas9 phagemids. DH5alpha(HP4_M13) [69] was 515 transformed with the GFPT phagemid (pCas9-GFPT-f1A or pCas9-GFPT-f1B) or the NT phagemid 516 (pCas9-GFPT-f1A or pCas9-GFPT-f1B) and plated on LB media containing carbenicillin and 517 kanamycin. Transformants were inoculated into 5 ml 2YT supplemented with 100 µg/ml carbenicillin 518 and 25 µg/ml kanamycin, incubated overnight, used 1-in-100 to seed 250 ml of the same media, 519 and incubated overnight. Cells were pelleted at 10,000×g for 15 minutes, the supernatant was 520 transferred to a new tube, 0.2 volumes of phage precipitation solution was added, and incubated 30 521 minutes on ice. Phage were pelleted at 20,000×g for 20 minutes with slow deceleration. The 522 supernatant was completely removed, phage were resuspended in PBS at 1% of the culture 523 volume, and glycerol was added to a final concentration of 10-15%. The phage solution was 524 centrifuged at 21,000×g to pellet insoluble matter, filtered through 0.45 µm, and stored at –80 °C. 525

Titration of M13 phage carrying phagemid DNA. Phage titer was determined using indicator 526 strain XL1-Blue MRF' or Sm^R W1655 F+. An overnight culture of the indicator strain in LB 527

supplemented with the appropriate antibiotics was subcultured 1-in-100 or 1-in-200 into fresh media and grown to an OD₆₀₀ of 0.8. To estimate titer, serial ten-fold dilutions of the phage preparation were made in PBS, and 10 µl of each dilution was used to infect 90 µl of cells. After incubating at 37 °C for 30 minutes with shaking, 10 µl of the infection mix was spotted onto LB supplemented with carbenicillin. For more accurate titration, 100 µl of phage dilutions were mixed with 900 µl cells in culture tubes, incubated at 37 °C for 30 minutes with shaking, and 100 µl was plated on LB carbenicillin.

Targeting experiments *in vitro* with M13 CRISPR-Cas9. Overnight cultures of fluorescently marked Sm^R W1655 F+ *sfgfp* and *mcherry* were prepared in LB supplemented with streptomycin, subcultured 1 in 200 into fresh media, and grown to an OD₆₀₀ of 0.8. 900 µl cells (approximately 1 × 10⁹) was transferred to a culture tube, 100 µl phage (approximately 1 × 10¹⁰ for f1A vectors and approximately 5 × 10¹⁰ for f1B vectors) was added, and the tube was incubated at 37 °C for 30 minutes. The infection culture was transferred to a microfuge tube, cells were pelleted at 21,000 × g for 1 minute, and the supernatant was removed. Cells were washed twice by adding 1 ml PBS, vortexing, pelleting cells, and removing supernatant. Cells were resuspended in 1 ml PBS, and ten-fold serially diluted in PBS. 10 µl of each dilution was spotted onto LB supplemented with carbenicillin and 100 µl was plated on larger plates for isolating single colonies for analysis. Colonies were picked and streak-purified four times to ensure phenotypic homogeneity and clonality.

Co-culture experiments with *sfgfp* and *mcherry* infected with M13 CRISPR-Cas9. Overnight cultures of fluorescently marked Sm^R W1655 F+ *sfgfp* and *mcherry* were prepared in LB supplemented with streptomycin. For each culture, three serial ten-fold dilutions were made in PBS, followed by a fourth ten-fold dilution into LB. Equal volumes of each were combined and 5 ml aliquots were transferred to culture tubes. Using a CFU assay, the input was determined to be

6×10^6 CFU of each strain or 1×10^7 CFU total. $10 \mu\text{l}$ (5×10^9) M13 carrying CRISPR-Cas9 was added, the co-culture was incubated at 37°C for 30 minutes, and carbenicillin was added to a final concentration of $100 \mu\text{g/ml}$. The co-culture was sampled for the $t = 0$ timepoint and then incubated for 24 hours with further sampling every 4 hours. At each timepoint, $200 \mu\text{l}$ was taken; $100 \mu\text{l}$ was used to assay carbenicillin in the media (see below) and the remaining $100 \mu\text{l}$ was used for plating as follows. To the $100 \mu\text{l}$ sample of culture, $900 \mu\text{l}$ was added and cells were washed by vortexing. Cells were pelleted by centrifuging at $21,000 \times g$ for 1 min, and $900 \mu\text{l}$ of the supernatant was removed. To remove residual phage and antibiotic, the wash was repeated once more by adding $900 \mu\text{l}$ PBS, vortexing, pelleting cells, and removing $900 \mu\text{l}$. Cells were resuspended in the remaining $100 \mu\text{l}$. Serial ten-fold dilutions were made in PBS and $10 \mu\text{l}$ of each dilution was spotted onto LB or LB carbenicillin.

Carbenicillin bioassay. Cultures were sampled over time, cells were pelleted at $21,000 \times g$ for 1 minute, and the supernatant was transferred to a new tube and frozen at -20°C until all timepoints were collected. The supernatants were thawed and assayed using a Kirby-Bauer disk diffusion test. An overnight culture of the indicator organism (*Bacillus subtilis* 168) was diluted in saline to an OD_{600} of 0.1. A cotton swab was dipped into this dilution and spread across LB agar, antibiotic sensitivity disks (Fisher Scientific S70150A) were overlaid using tweezers, and $20 \mu\text{l}$ of the supernatant was applied to the disk. At the same time, carbenicillin standards were prepared from $1 \mu\text{g/ml}$ to $100 \mu\text{g/ml}$ and also applied to discs. Plates were incubated overnight at 37°C and imaged the following morning.

Treatment of mice with phage. Filtered phage solutions stored at -80°C were thawed and used directly. Unfiltered phage solutions were precipitated by diluting approximately 5-fold in PBS, adding 0.2 volumes phage precipitation solution, incubating for 15 minutes on ice, pelleting at $15,000$ – $21,000 \times g$ for 15 minutes at 4°C , resuspending in PBS, centrifuging to pellet insoluble

matter, and filtering through 0.45 μm . Heat-inactivated phage were prepared by incubating 1 ml 576
aliquots at 95 °C in a water bath for 30 minutes. Streptomycin-treated mice colonized with Sm^R 577
E. coli were orally gavaged with 0.2 ml of phage and placed on drinking water containing both 578
streptomycin and carbenicillin. 579

Flow cytometry. For turbid *in vitro* cultures, samples were diluted 1 in 10,000 in PBS. For mouse 580
fecal pellets, samples were used fresh or thawed from -80 °C, and suspended in 500 μl PBS by 581
manual mixing and vortexing. Fecal suspensions were incubated aerobically at 4 °C overnight to 582
improve fluorescence signal (Figure S17). Samples were vortexed to mix, large particulate matter 583
was pelleted by centrifuging at 100 \times g for 30 seconds, and the sample was diluted 1-in-100 in PBS. 584
Samples were run on a BD LSRFortessa DUAL flow cytometer using a 530/30 nm filter for GFP 585
fluorescence and 610/20 nm for mCherry fluorescence, with the following voltages: 750 V for FSC, 586
400 V for SSC, 700 V for mCherry, and 700-800 V (*in vivo*) or 650 V (*in vitro*) for GFP. Flow 587
cytometry data were analyzed in R using packages *flowCore* v1.52.1 [80], *Phenoflow* v1.1.2 [81], 588
and *ggcyto* v1.14.0 [82]. Typically, between 10,000 and 100,000 events were collected per sample, 589
and data were rarefied after gating on FSC and SSC. 590

Analysis of plasmid DNA and genomic DNA from *in vitro* or *in vivo* isolates. Fecal 591
suspensions in PBS or saline were cultured on LB or Difco MacConkey agar plates supplemented 592
with the appropriate antibiotics. Colonies were picked, streak-purified, and inoculated into LB or TB 593
supplemented with the appropriate antibiotics. Plasmid DNA was extracted using a QIAprep Spin 594
Miniprep Kit (Qiagen 27106), eluted in TE buffer, and incubated at 60 °C for 10 minutes. Samples 595
were quantified using a NanoDrop One spectrophotometer and 200-600 ng was digested with 596
FastDigest restriction enzymes (KpnI, Thermo Scientific FD0524; XbaI, Thermo Scientific FD0684) 597
for 10 minutes at 37 °C followed by gel electrophoresis. Spacer sequences on phagemids were 598
confirmed by Sanger sequencing using primer PSP108. Genomic DNA was extracted crudely to 599

use as template for PCR. Briefly, 1.5 ml to 3 ml of culture was transferred to a microfuge tube, cells 600
were pelleted by centrifuging, and the supernatant was discarded. The pellet was frozen, allowed 601
to thaw on ice, resuspended in 100 μ l TE, and incubated at 100 °C for 15 minutes in an Eppendorf 602
ThermoMixer. Samples were cooled on ice, cell debris was pelleted by centrifuging at 21,000 \times g for 603
1 minute, the supernatant was transferred to a new tube, and diluted 1-in-100 in TE to use as 604
template DNA. PCR was performed using KOD Hot Start DNA polymerase (Millipore 71842-3) 605
using primers KL207 and KL200 for PCR of the *sfgfp* gene and primers BAC338F and BAC805R 606
for the 16S rRNA gene [83]. 607

References

1. Shepherd, E. S., DeLoache, W. C., Pruss, K. M., Whitaker, W. R. & Sonnenburg, J. L. An exclusive metabolic niche enables strain engraftment in the gut microbiota. *Nature* **557**, 434–438 (2018).
2. Kearney, S. M., Gibbons, S. M., Erdman, S. E. & Alm, E. J. Orthogonal dietary niche enables reversible engraftment of a gut bacterial commensal. *Cell Rep.* **24**, 1842–1851 (2018).
3. Staley, C. *et al.* Stable engraftment of human microbiota into mice with a single oral gavage following antibiotic conditioning. *Microbiome* **5**, 87 (2017).
4. Thompson, J. A., Oliveira, R. A., Djukovic, A., Ubeda, C. & Xavier, K. B. Manipulation of the quorum sensing signal AI-2 affects the antibiotic-treated gut microbiota. *Cell Rep.* **10**, 1861–1871 (2015).
5. Isabella, V. M. *et al.* Development of a synthetic live bacterial therapeutic for the human metabolic disease phenylketonuria. *Nat. Biotechnol.* **36**, 857–864 (2018).
6. Kurtz, C. B. *et al.* An engineered e. coli nissle improves hyperammonemia and survival in mice and shows dose-dependent exposure in healthy humans. *Sci. Transl. Med.* **11** (2019).
7. Zhu, W. *et al.* Precision editing of the gut microbiota ameliorates colitis. *Nature* **553**, 208–211 (2018).
8. Wallace, B. D. *et al.* Alleviating cancer drug toxicity by inhibiting a bacterial enzyme. *Science* **330**, 831–835 (2010).
9. Mimee, M., Tucker, A. C., Voigt, C. A. & Lu, T. K. Programming a human commensal bacterium, *Bacteroides thetaiotaomicron*, to sense and respond to stimuli in the murine gut microbiota. *Cell Systems* **1**, 62–71 (2015).
10. Lim, B., Zimmermann, M., Barry, N. A. & Goodman, A. L. Engineered regulatory systems modulate gene expression of human commensals in the gut. *Cell* **169**, 547–558.e15 (2017).
11. Ronda, C., Chen, S. P., Cabral, V., Yaung, S. J. & Wang, H. H. Metagenomic engineering of the mammalian gut microbiome in situ. *Nat. Methods* **16**, 167–170 (2019).
12. Rodrigues, M., McBride, S. W., Hullahalli, K., Palmer, K. L. & Duerkop, B. A. Conjugative delivery of CRISPR-Cas9 for the selective depletion of antibiotic-resistant enterococci. *Antimicrob. Agents Chemother.* AAC.01454–19 (2019).
13. Merril, C. R., Scholl, D. & Adhya, S. L. The prospect for bacteriophage therapy in western medicine. *Nat. Rev. Drug Discov.* **2**, 489–497 (2003).
14. Abedon, S. T., Kuhl, S. J., Blasdel, B. G. & Kutter, E. M. Phage treatment of human infections. *Bacteriophage* **1**, 66–85 (2011).
15. Lu, T. K. & Koeris, M. S. The next generation of bacteriophage therapy. *Curr. Opin. Microbiol.* **14**, 524–531 (2011).

16. Brüssow, H. Phage therapy for the treatment of human intestinal bacterial infections: soon to be a reality? *Expert Rev. Gastroenterol. Hepatol.* **11**, 785–788 (2017).
17. Abedon, S. T., García, P., Mullany, P. & Aminov, R. Editorial: Phage therapy: Past, present and future. *Front. Microbiol.* **8**, 981 (2017).
18. Maura, D. *et al.* Intestinal colonization by enteroaggregative escherichia coli supports long-term bacteriophage replication in mice. *Environ. Microbiol.* **14**, 1844–1854 (2012).
19. Weiss, M. *et al.* In vivo replication of T4 and T7 bacteriophages in germ-free mice colonized with escherichia coli. *Virology* **393**, 16–23 (2009).
20. Chibani-Chennoufi, S. *et al.* In vitro and in vivo bacteriolytic activities of escherichia coli phages: implications for phage therapy. *Antimicrob. Agents Chemother.* **48**, 2558–2569 (2004).
21. Maura, D., Galtier, M., Le Bouguéneq, C. & Debarbieux, L. Virulent bacteriophages can target O104:H4 enteroaggregative escherichia coli in the mouse intestine. *Antimicrob. Agents Chemother.* **56**, 6235–6242 (2012).
22. Porter, N. T. *et al.* Phase-variable capsular polysaccharides and lipoproteins modify bacteriophage susceptibility in bacteroides thetaiotaomicron (2020).
23. Citorik, R. J., Mimee, M. & Lu, T. K. Sequence-specific antimicrobials using efficiently delivered RNA-guided nucleases. *Nat. Biotechnol.* **32**, 1141–1145 (2014).
24. Bikard, D. *et al.* Exploiting CRISPR-Cas nucleases to produce sequence-specific antimicrobials. *Nat. Biotechnol.* **32**, 1146–1150 (2014).
25. Park, J. Y. *et al.* Genetic engineering of a temperate phage-based delivery system for CRISPR/Cas9 antimicrobials against staphylococcus aureus. *Sci. Rep.* **7**, 44929 (2017).
26. Selle, K. *et al.* In vivo targeting of clostridioides difficile using Phage-Delivered CRISPR-Cas3 antimicrobials. *MBio* **11** (2020).
27. Shkoporov, A. N. & Hill, C. Bacteriophages of the human gut: The “known unknown” of the microbiome. *Cell Host Microbe* **25**, 195–209 (2019).
28. Reyes, A., Semenkovich, N. P., Whiteson, K., Rohwer, F. & Gordon, J. I. Going viral: next-generation sequencing applied to phage populations in the human gut. *Nat. Rev. Microbiol.* **10**, 607–617 (2012).
29. Brüssow, H. Environmental microbiology: Too much food for thought? - an argument for reductionism. *Environ. Microbiol.* (2018).
30. Hofschneider, P. H. Untersuchungen über kleine“ e. coli K 12 bakterioophagen. *Zeitschrift für Naturforschung B* **18**, 203–210 (1963).
31. Ackermann, H.-W. Phage classification and characterization. *Methods Mol. Biol.* **501**, 127–140 (2009).
32. Salivar, W. O., Tzagoloff, H. & Pratt, D. Some Physical-Chemical and biological properties of the Rod-Shaped coliphage M13. *Virology* **24**, 359–371 (1964).

33. Lee, G. S. & Ames, G. F. Analysis of promoter mutations in the histidine transport operon of salmonella typhimurium: use of hybrid M13 bacteriophages for cloning, transformation, and sequencing. *J. Bacteriol.* **159**, 1000–1005 (1984).
34. Lin, A. *et al.* Inhibition of bacterial conjugation by phage M13 and its protein g3p: quantitative analysis and model. *PLoS One* **6**, e19991 (2011).
35. Yanisch-Perron, C., Vieira, J. & Messing, J. Improved M13 phage cloning vectors and host strains: nucleotide sequences of the m13mp18 and pUC19 vectors. *Gene* **33**, 103–119 (1985).
36. Sanger, F., Coulson, A. R., Barrell, B. G., Smith, A. J. & Roe, B. A. Cloning in single-stranded bacteriophage as an aid to rapid DNA sequencing. *J. Mol. Biol.* **143**, 161–178 (1980).
37. Zoller, M. J. & Smith, M. Oligonucleotide-directed mutagenesis using m13-derived vectors: an efficient and general procedure for the production of point mutations in any fragment of DNA. *Nucleic Acids Res.* **10**, 6487–6500 (1982).
38. Smith, G. P. & Petrenko, V. A. Phage display. *Chem. Rev.* **97**, 391–410 (1997).
39. Sidhu, S. S. Engineering M13 for phage display. *Biomol. Eng.* **18**, 57–63 (2001).
40. Roux, S. *et al.* Cryptic inoviruses revealed as pervasive in bacteria and archaea across earth's biomes. *Nature Microbiology* **4**, 1895–1906 (2019).
41. Pasqualini, R. & Ruoslahti, E. Organ targeting in vivo using phage display peptide libraries. *Nature* **380**, 364–366 (1996).
42. Rajotte, D. *et al.* Molecular heterogeneity of the vascular endothelium revealed by in vivo phage display. *J. Clin. Invest.* **102**, 430–437 (1998).
43. Krag, D. N. *et al.* Phage-displayed random peptide libraries in mice: toxicity after serial panning. *Cancer Chemother. Pharmacol.* **50**, 325–332 (2002).
44. Westwater, C. *et al.* Use of genetically engineered phage to deliver antimicrobial agents to bacteria: an alternative therapy for treatment of bacterial infections. *Antimicrob. Agents Chemother.* **47**, 1301–1307 (2003).
45. Lu, T. K. & Collins, J. J. Engineered bacteriophage targeting gene networks as adjuvants for antibiotic therapy. *Proc. Natl. Acad. Sci. U. S. A.* **106**, 4629–4634 (2009).
46. Cao, J. *et al.* Helicobacter pylori-antigen-binding fragments expressed on the filamentous M13 phage prevent bacterial growth. *Biochim. Biophys. Acta* **1474**, 107–113 (2000).
47. Miller, C. P. & Bohnhoff, M. Changes in the mouse's enteric microflora associated with enhanced susceptibility to salmonella infection following streptomycin treatment. *J. Infect. Dis.* **113**, 59–66 (1963).
48. Myhal, M. L., Laux, D. C. & Cohen, P. S. Relative colonizing abilities of human fecal and K 12 strains of escherichia coli in the large intestines of streptomycin-treated mice. *Eur. J. Clin. Microbiol.* **1**, 186–192 (1982).

49. Leatham, M. P. *et al.* Precolonized human commensal escherichia coli strains serve as a barrier to e. coli O157:H7 growth in the streptomycin-treated mouse intestine. *Infect. Immun.* **77**, 2876–2886 (2009).
50. Altling-Mees, M. A. & Short, J. M. pbluescript II: gene mapping vectors. *Nucleic Acids Res.* **17**, 9494 (1989).
51. Kimura, T. & Higaki, K. Gastrointestinal transit and drug absorption. *Biol. Pharm. Bull.* **25**, 149–164 (2002).
52. Coste, M., Gouet, P. & Escoula, L. Ampicillin inactivation in the caecum of axenic, gnotoxenic and conventional lambs: interaction with resistant or sensitive escherichia coli. *J. Gen. Microbiol.* **130**, 1325–1330 (1984).
53. van der Waaij, D., de Vries-Hospers, H. G. & Welling, G. W. The influence of antibiotics on gut colonization. *J. Antimicrob. Chemother.* **18 Suppl C**, 155–158 (1986).
54. Corpet, D. E., Lumeau, S. & Corpet, F. Minimum antibiotic levels for selecting a resistance plasmid in a gnotobiotic animal model. *Antimicrob. Agents Chemother.* **33**, 535–540 (1989).
55. Reikvam, D. H. *et al.* Depletion of murine intestinal microbiota: effects on gut mucosa and epithelial gene expression. *PLoS One* **6**, e17996 (2011).
56. Duval-Iflah, Y., Raibaud, P., Tancrede, C. & Rousseau, M. R-plasmic transfer from serratia liquefaciens to escherichia coli in vitro and in vivo in the digestive tract of gnotobiotic mice associated with human fecal flora. *Infect. Immun.* **28**, 981–990 (1980).
57. Jończyk, E., Kłak, M., Miedzybrodzki, R. & Górski, A. The influence of external factors on bacteriophages—review. *Folia Microbiol.* **56**, 191–200 (2011).
58. Tóthová, L., Bábíčková, J. & Celec, P. Phage survival: the biodegradability of M13 phage display library in vitro. *Biotechnol. Appl. Biochem.* **59**, 490–494 (2012).
59. Jiang, W., Bikard, D., Cox, D., Zhang, F. & Marraffini, L. A. RNA-guided editing of bacterial genomes using CRISPR-Cas systems. *Nat. Biotechnol.* **31**, 233–239 (2013).
60. Cui, L. & Bikard, D. Consequences of cas9 cleavage in the chromosome of escherichia coli. *Nucleic Acids Res.* **44**, 4243–4251 (2016).
61. Gynnå, A. H., Wiktor, J., Leroy, P. & Elf, J. RecA mediated homology search finds segregated sister locus in minutes after a double stranded break (2020).
62. Yosef, I., Manor, M., Kiro, R. & Qimron, U. Temperate and lytic bacteriophages programmed to sensitize and kill antibiotic-resistant bacteria. *Proceedings of the National Academy of Sciences* **112**, 201500107 (2015).
63. Bikard, D. & Barrangou, R. Using CRISPR-Cas systems as antimicrobials. *Curr. Opin. Microbiol.* **37**, 155–160 (2017).
64. Bethesda Research Laboratories. BRL pUC host: *E. coli* DH5 α competent cells. *Focus* **8**, 8 (1986).

65. Bachmann, B. J. Derivations and genotypes of some mutant derivatives of *Escherichia coli* K-12. In Neidhardt, F. C. e. a. (ed.) *Escherichia coli and Salmonella typhimurium: Cellular and Molecular Biology* (ASM Press, Washington, DC, 1996).
66. Vigouroux, A., Oldewurtel, E., Cui, L., Bikard, D. & van Teeffelen, S. Tuning dCas9's ability to block transcription enables robust, noiseless knockdown of bacterial genes. *Mol. Syst. Biol.* **14**, e7899 (2018).
67. Jensen, S. I., Lennen, R. M., Herrgård, M. J. & Nielsen, A. T. Seven gene deletions in seven days: Fast generation of *Escherichia coli* strains tolerant to acetate and osmotic stress. *Sci. Rep.* **5**, 17874 (2015).
68. St-Pierre, F. *et al.* One-step cloning and chromosomal integration of DNA. *ACS Synth. Biol.* **2**, 537–541 (2013).
69. Praetorius, F. *et al.* Biotechnological mass production of DNA origami. *Nature* **552**, 84–87 (2017).
70. Gohl, D. M. *et al.* Systematic improvement of amplicon marker gene methods for increased accuracy in microbiome studies. *Nat. Biotechnol.* **34**, 942–949 (2016).
71. Bisanz, J. 16S rRNA amplicon sequencing pipeline. https://github.com/jbisanz/16Spipelines/blob/master/QIIME2_pipeline.Rmd.
72. Bolyen, E. *et al.* Reproducible, interactive, scalable and extensible microbiome data science using QIIME 2. *Nat. Biotechnol.* **37**, 852–857 (2019).
73. Callahan, B. J. *et al.* DADA2: High-resolution sample inference from illumina amplicon data. *Nat. Methods* **13**, 581–583 (2016).
74. Bisanz, J. qiime2r. <https://github.com/jbisanz/qiime2R>.
75. McMurdie, P. J. & Holmes, S. phyloseq: an R package for reproducible interactive analysis and graphics of microbiome census data. *PLoS One* **8**, e61217 (2013).
76. Smith, S. D. phyloSMITH: an R-package for reproducible and efficient microbiome analysis with phyloseq-objects. *Journal of Open Source Software* **4**, 1442 (2019).
77. Datsenko, K. a. & Wanner, B. L. One-step inactivation of chromosomal genes in *Escherichia coli* K-12 using PCR products. *Proc. Natl. Acad. Sci. U. S. A.* **97**, 6640–6645 (2000).
78. Timms, A. R., Steingrimsdottir, H., Lehmann, A. R. & Bridges, B. A. Mutant sequences in the *rpsL* gene of *Escherichia coli* b/r: mechanistic implications for spontaneous and ultraviolet light mutagenesis. *Mol. Gen. Genet.* **232**, 89–96 (1992).
79. Tonikian, R., Zhang, Y., Boone, C. & Sidhu, S. S. Identifying specificity profiles for peptide recognition modules from phage-displayed peptide libraries. *Nat. Protoc.* **2**, 1368–1386 (2007).
80. Hahne, F. *et al.* flowcore: a bioconductor package for high throughput flow cytometry. *BMC Bioinformatics* **10**, 106 (2009).

81. Props, R., Monsieurs, P., Mysara, M., Clement, L. & Boon, N. Measuring the biodiversity of microbial communities by flow cytometry. *Methods Ecol. Evol.* **7**, 1376–1385 (2016).
82. Van, P., Jiang, W., Gottardo, R. & Finak, G. ggcyto: next generation open-source visualization software for cytometry. *Bioinformatics* **34**, 3951–3953 (2018).
83. Yu, Y., Lee, C., Kim, J. & Hwang, S. Group-specific primer and probe sets to detect methanogenic communities using quantitative real-time polymerase chain reaction. *Biotechnol. Bioeng.* **89**, 670–679 (2005).

Supplementary Figures

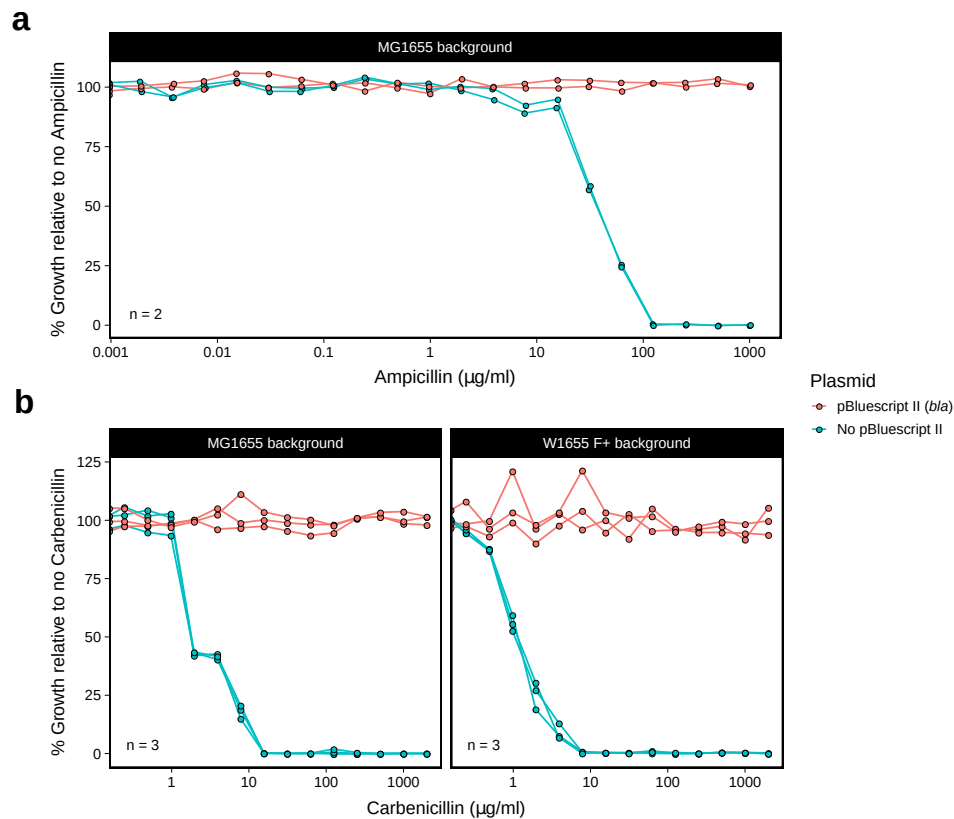


Figure S1. Minimum inhibitory concentration (MIC) assays. (a) The plasmid pBluescript II confers resistance to ampicillin exceeding 1 mg/ml in the *E. coli* MG1655 background. In the absence of the plasmid, the MIC is approximately 100 $\mu\text{g/ml}$. (b) pBluescript II confers resistance to carbenicillin exceeding 2 mg/ml in both the *E. coli* MG1655 and W1655 F+ backgrounds. In the absence of the plasmid, the same strains have an MIC of approximately 10 $\mu\text{g/ml}$. bla, beta-lactamase.

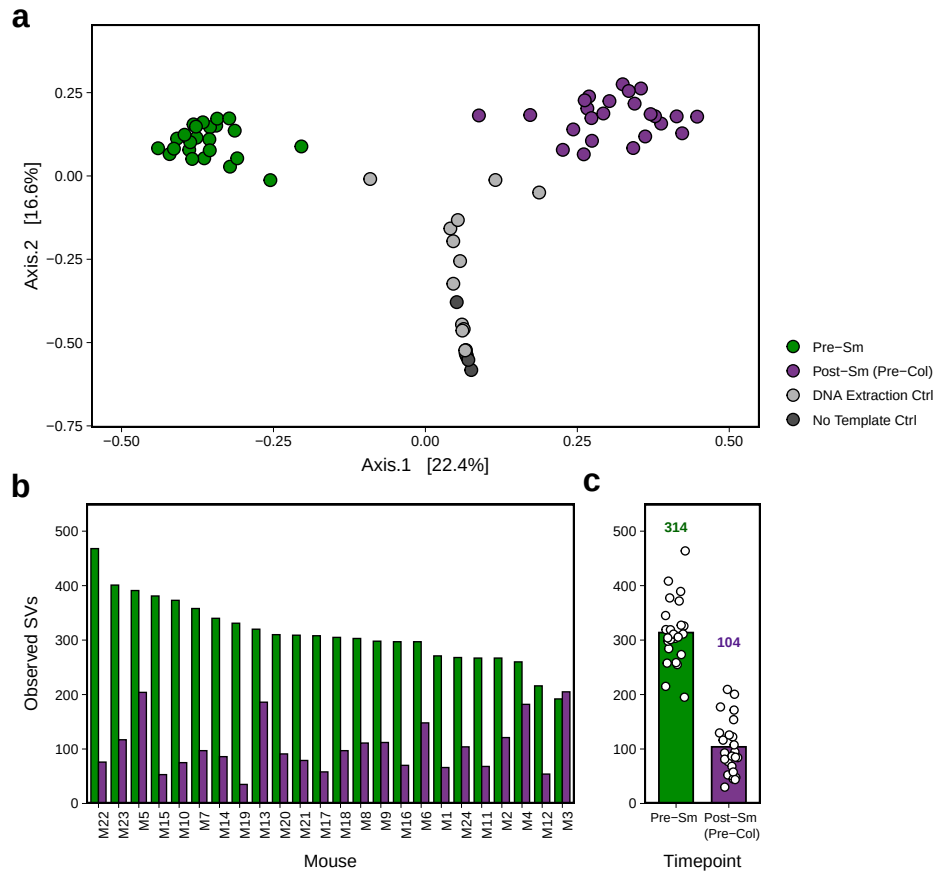


Figure S2. Streptomycin (Sm) treatment reduces bacterial diversity in mice. (a) Principle coordinate analysis (Bray-Curtis) indicates that pre-Sm and post-Sm fecal samples are distinct. (b) In a cohort of 24 individually caged mice, Sm treatment generally leads to a decrease in the number of observed 16S rRNA gene sequence variants (SVs) relative to pre-treatment. (c) The mean number of observed SVs pre-Sm was 314 while the mean post-Sm (before colonizing with Sm^R *E. coli*) was 104.

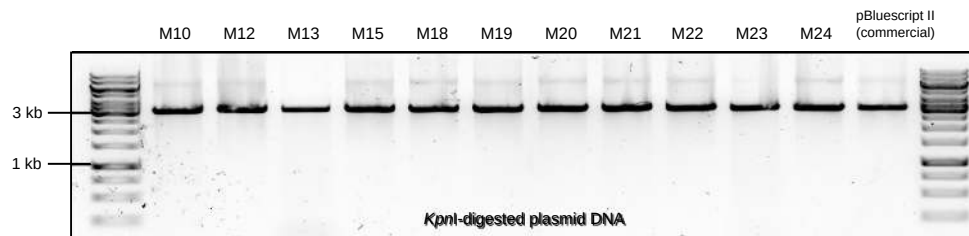


Figure S3. Diagnostic digest of plasmid DNA recovered from *E. coli* in the gut post phage delivery. Plasmid DNA was recovered from Carb^R colonies isolated from the feces of the 11 mice that were successfully colonized during carbenicillin treatment (Figure 1d); DNA was digested with the restriction enzyme KpnI for comparison to linearized 3-kb pBluescript II.

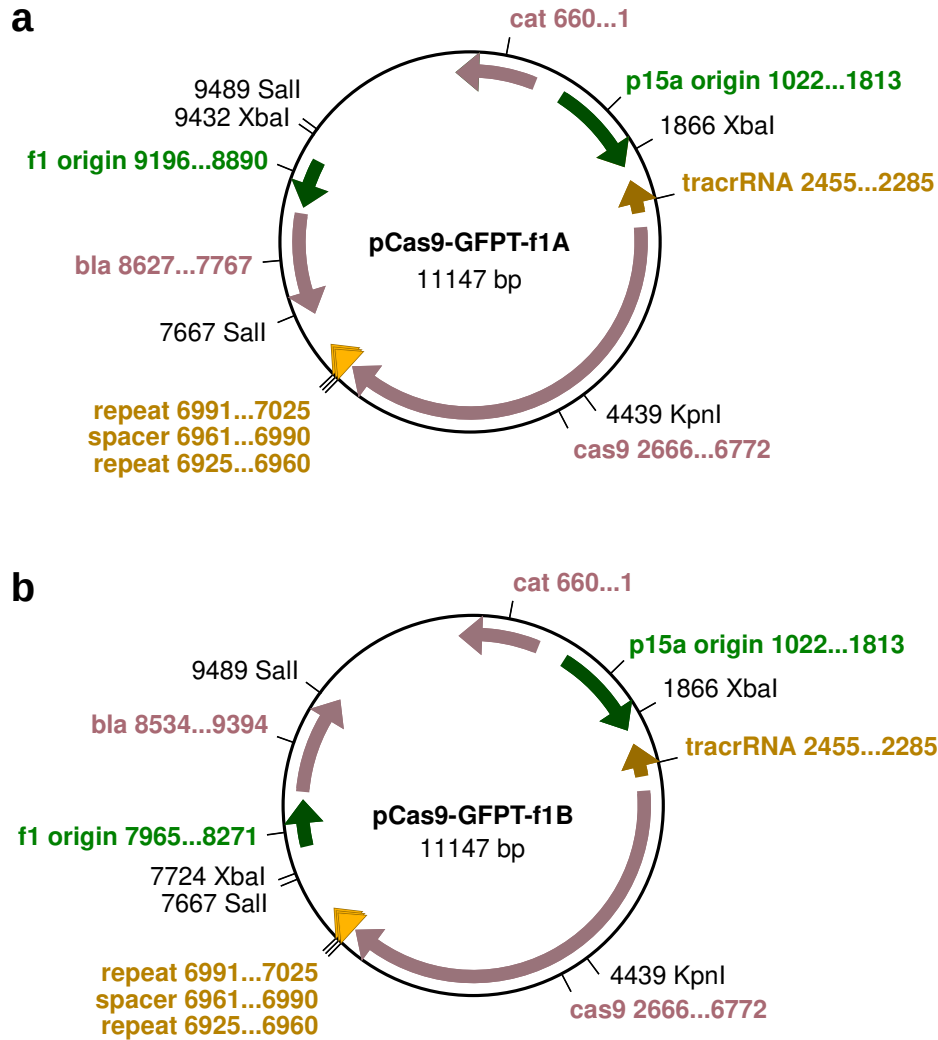


Figure S4. Plasmid maps of GFP-targeting (GFPT) CRISPR-Cas9 vectors. The non-targeting (NT) versions of these vectors (not shown here) are identical to the GFPT vectors except in the spacer sequence. The f1-*bla* fragment was cloned as a Sall fragment in both possible orientations for either strand of DNA to be packaged into M13 phage. **(a)** The first orientation is designated f1A. **(b)** The second orientation is designated f1B. cat, chloramphenicol acetyltransferase (Cm^R); bla, beta-lactamase ($Carb^R$).

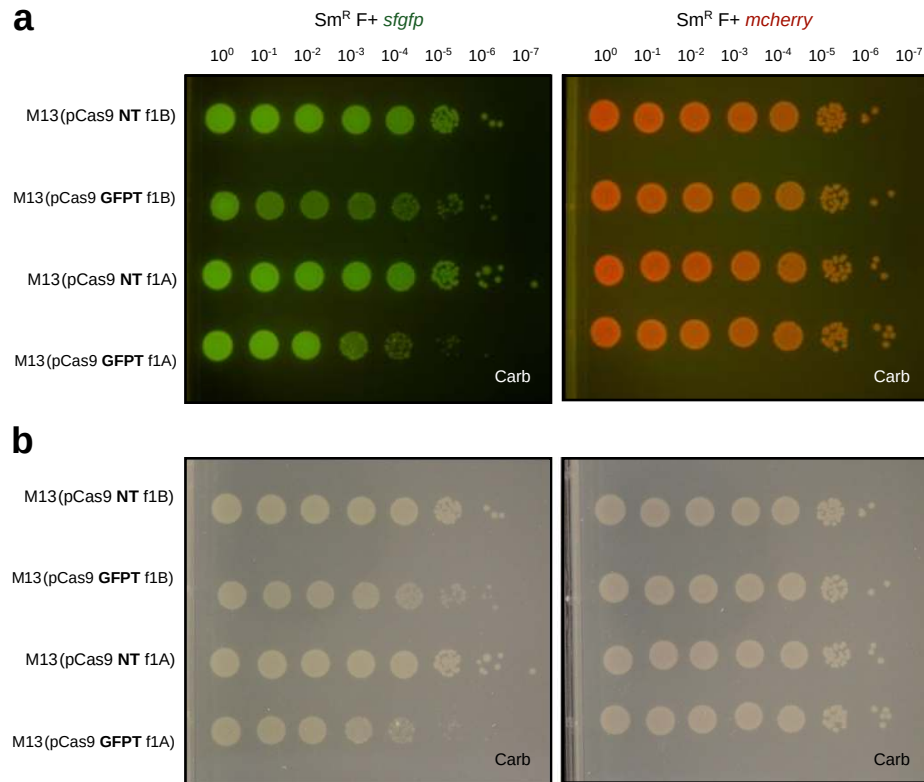


Figure S5. GFP-marked *E. coli* exhibits impaired colony growth after infection with M13 carrying GFP-targeting CRISPR-Cas9. The GFP-marked and mCherry-marked derivatives of Sm^R *E. coli* W6555 F+ were infected with NT M13 or GFPT M13. **(a)** Growth impairment of the GFP-marked strain under GFPT conditions was evident under blue light. **(b)** Impaired colonies exhibited a translucent quality that was more pronounced under white light.

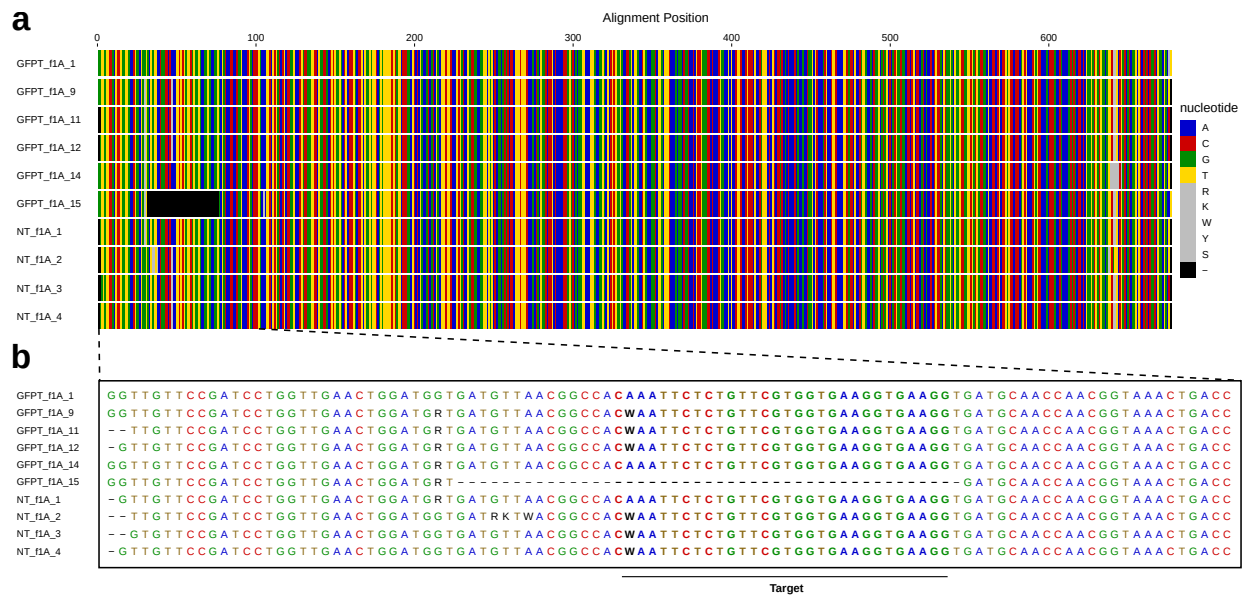


Figure S7. Analysis of *sfGFP* gene from streak-purified clones post M13 targeting *in vitro*. (a) Sanger sequencing of the *sfGFP* PCR amplicons (Figure 2c) confirmed the partial loss observed for clone 15 by gel electrophoresis. (b) Pullout: the lost region of the *sfGFP* coding sequence encompasses CRISPR-Cas9 target site.

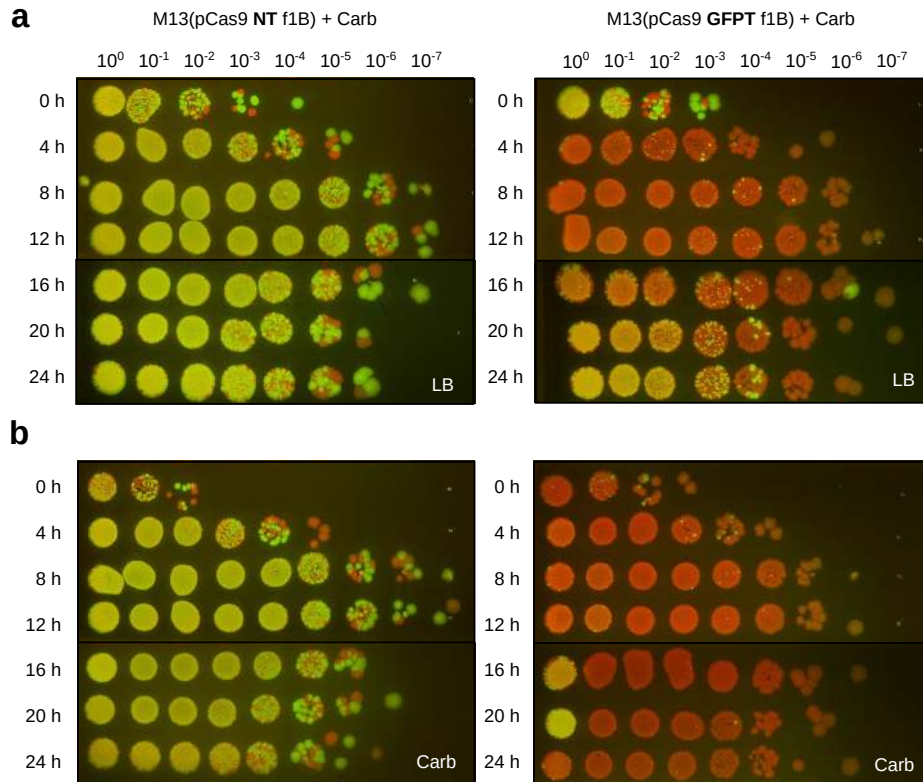


Figure S8. Recovery of GFP+ cells at later timepoints in *in vitro* co-cultures of *sfGFP* and *mCherry E. coli* F+ after infection with GFPT M13 is likely due to lack of selection for CRISPR-Cas9 phagemid. (a) On non-selective media, GFP fluorescent colonies are detected at later timepoints of the co-culture infected with GFPT M13. (b) Lack of GFP fluorescent colonies after testing the same co-culture on media with carbenicillin indicates that those GFP+ colonies at later timepoints derives from cells that are Carb^S and suggests that they do not harbour the CRISPR-Cas9 phagemid.

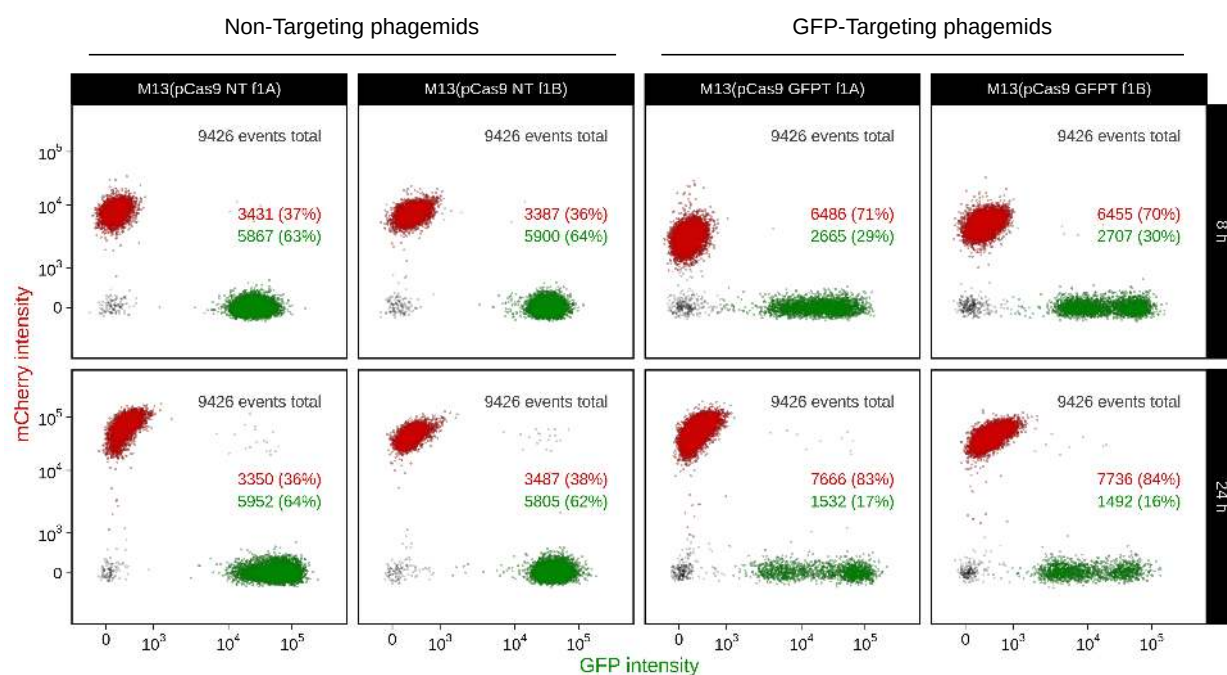


Figure S9. Flow cytometry on co-cultures at 8 h and 24 h after addition of NT M13 or GFPT M13 shows decreased relative abundance of the GFP strain under targeting conditions. Co-cultures of GFP-marked and mCherry-marked *E. coli* F+ were infected with phage and carbenicillin was added to select for phage infection. The relative abundance of GFP+ events is decreased in GFPT conditions at 8 h and further decreased by 24 h. Non-targeting phagemids are pCas9-NT-f1A and pCas9-NT-f1B; GFP-targeting phagemids are pCas9-GFPT-f1A and pCas9-GFPT-f1B.

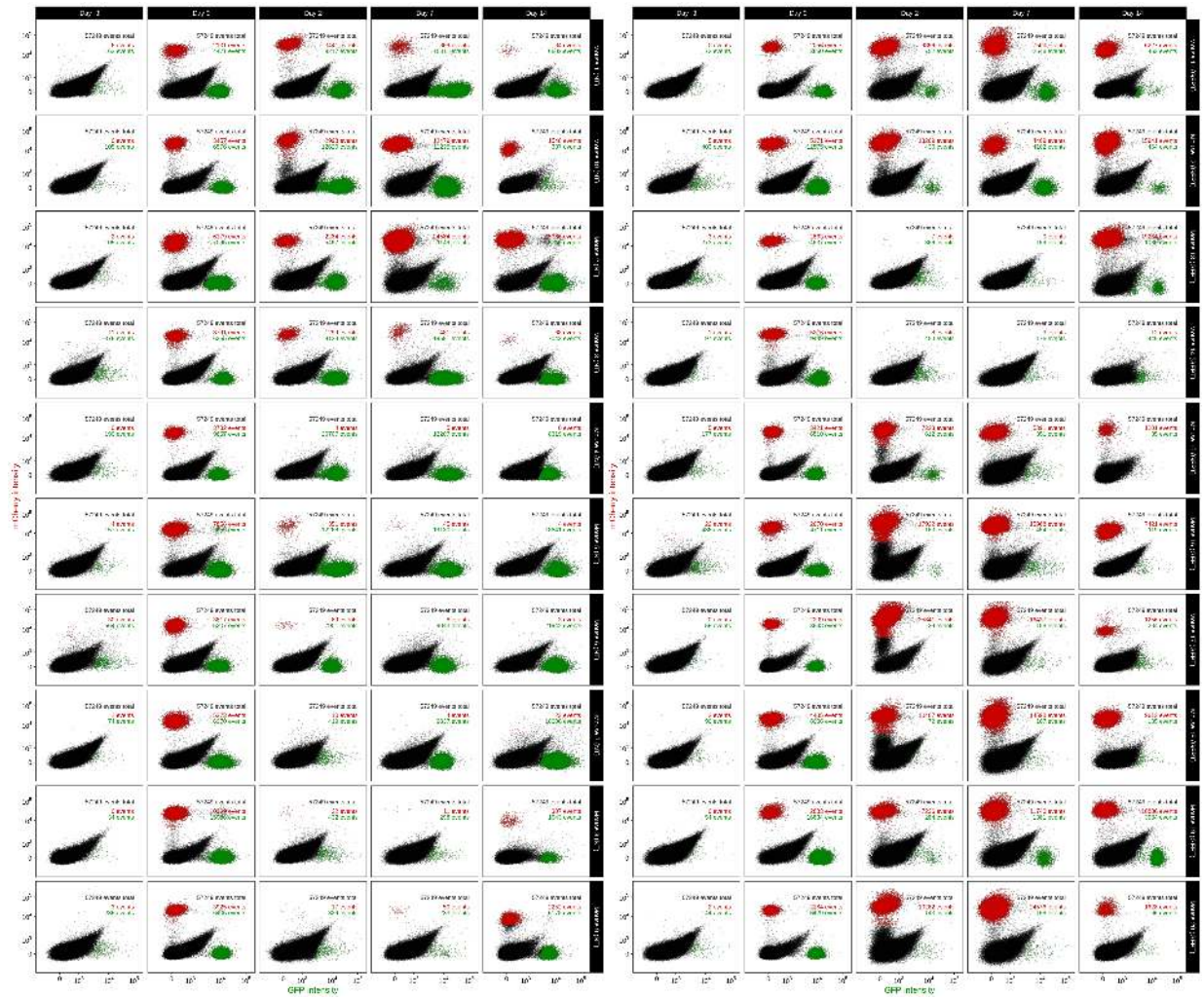


Figure S10. Flow cytometry plots of fecal samples for *in vivo* competition of GFP-marked and mCherry-marked *E. coli* under NT or GFPT conditions for all mice at all timepoints. Mice ($n = 10$ per group) were given either NT M13 (left) or GFPT M13 (right). Day -3, before engrafting *E. coli*; Day 0, after engraftment with both GFP+ and mCherry+ strains; Day -2, post phage and carbenicillin treatment; Day 7, one week post-phage and carbenicillin; Day -14, one week after removing carbenicillin from drinking water.

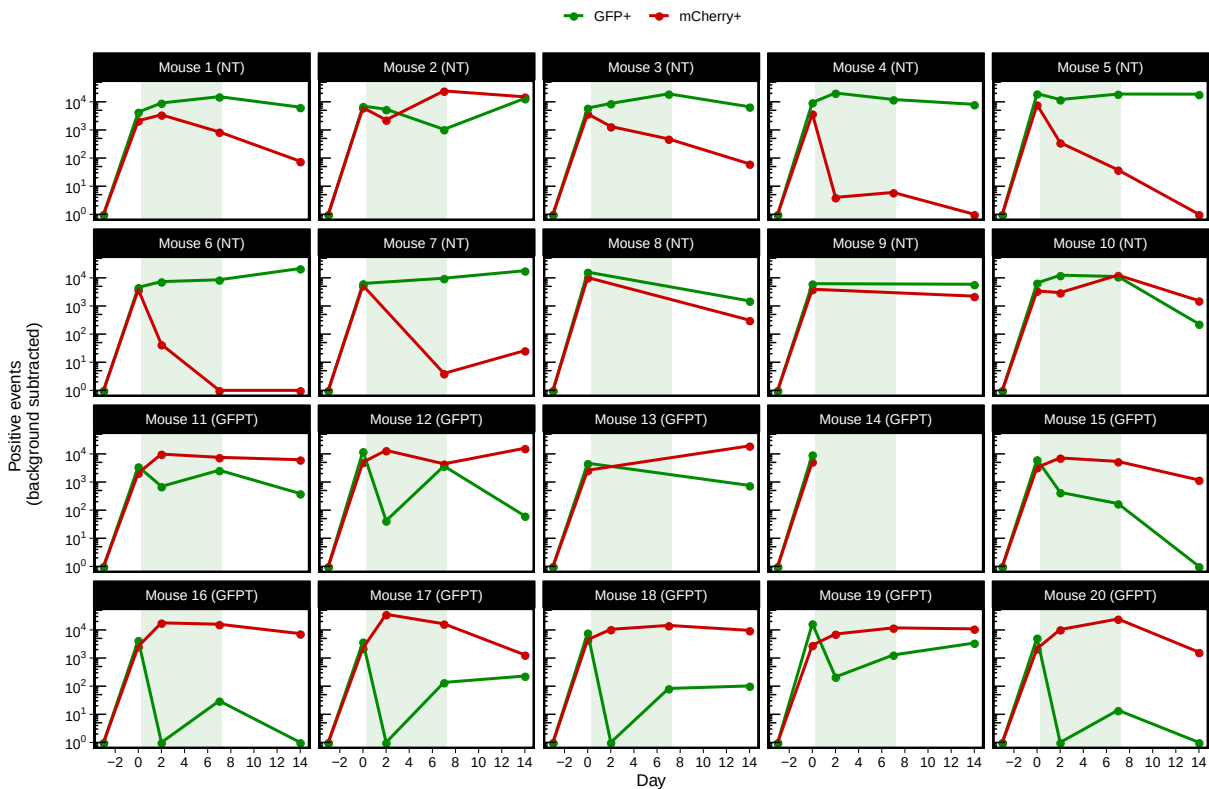


Figure S11. GFP+ and mCherry+ events by flow cytometry in fecal samples over time for individual mice in *in vivo* competition of GFP-marked and mCherry-marked *E. coli* under NT or GFPT conditions. Mice were treated with either NT M13 (M1 to M10) or GFPT M13 (M11 to M20). For each mouse, the number of positive events on Day -3 (before *E. coli* engraftment) was used to subtract background for all subsequent timepoints. Shaded green area indicates duration of carbenicillin treatment. Timepoints were excluded when both mCherry+ and GFP+ events were below background thresholds, calculated as the respective highest observed background on Day -3 multiplied by a factor of 3.

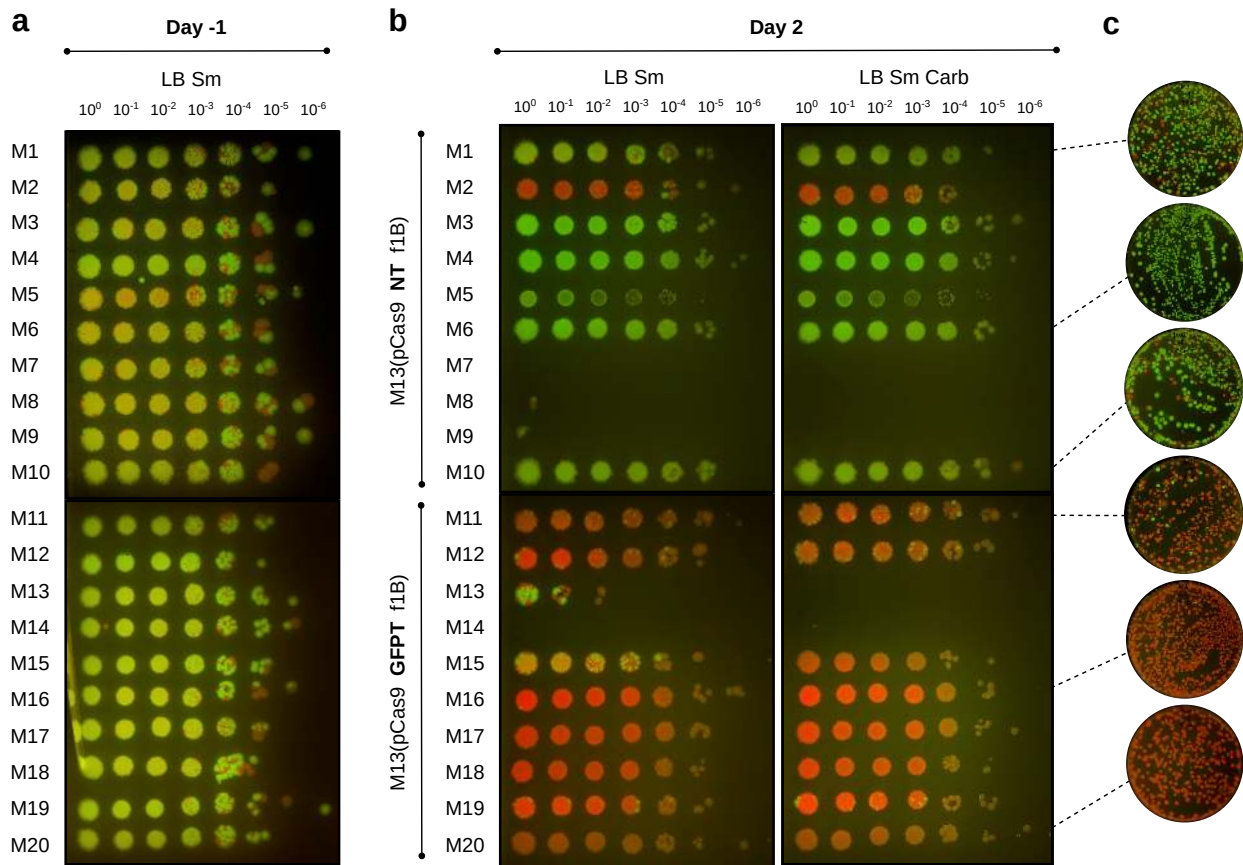


Figure S12. Culturing from fecal samples of mice before (Day -1) or after treatment (Day 2) with NT M13 or GFPT M13 in *in vivo* competition of GFP-marked and mCherry-marked Sm^R *E. coli* F+. (a) At Day -1, engraftment of both the GFP+ and mCherry+ *E. coli* was confirmed in fecal samples of all mice by culturing on LB with streptomycin. (b) After treating with NT M13 (M1 to M10) or GFPT M13 (M11 to M20) and carbenicillin to select for phage infection, culture of *E. coli* on LB streptomycin (Sm) from fecal samples on Day -2 of GFPT mice exhibit decreased GFP fluorescence. Culturing from the same samples on LB with both streptomycin and carbenicillin (Carb) suggests that for some mice, fluorescent colonies arising on LB streptomycin are Carb^S, *i.e.*, that they do not carry the CRISPR-Cas9 phagemid. Lack of fluorescent *E. coli* in fecal samples indicates eradication by carbenicillin where phage infection leading to colonization by Carb^R *E. coli* has not occurred. (c) Day 2 fecal suspensions from a subset of the mice (M1, M6, M10 for NT; M11, M16, M20 for GFPT) were cultured on larger plates for confirmation.

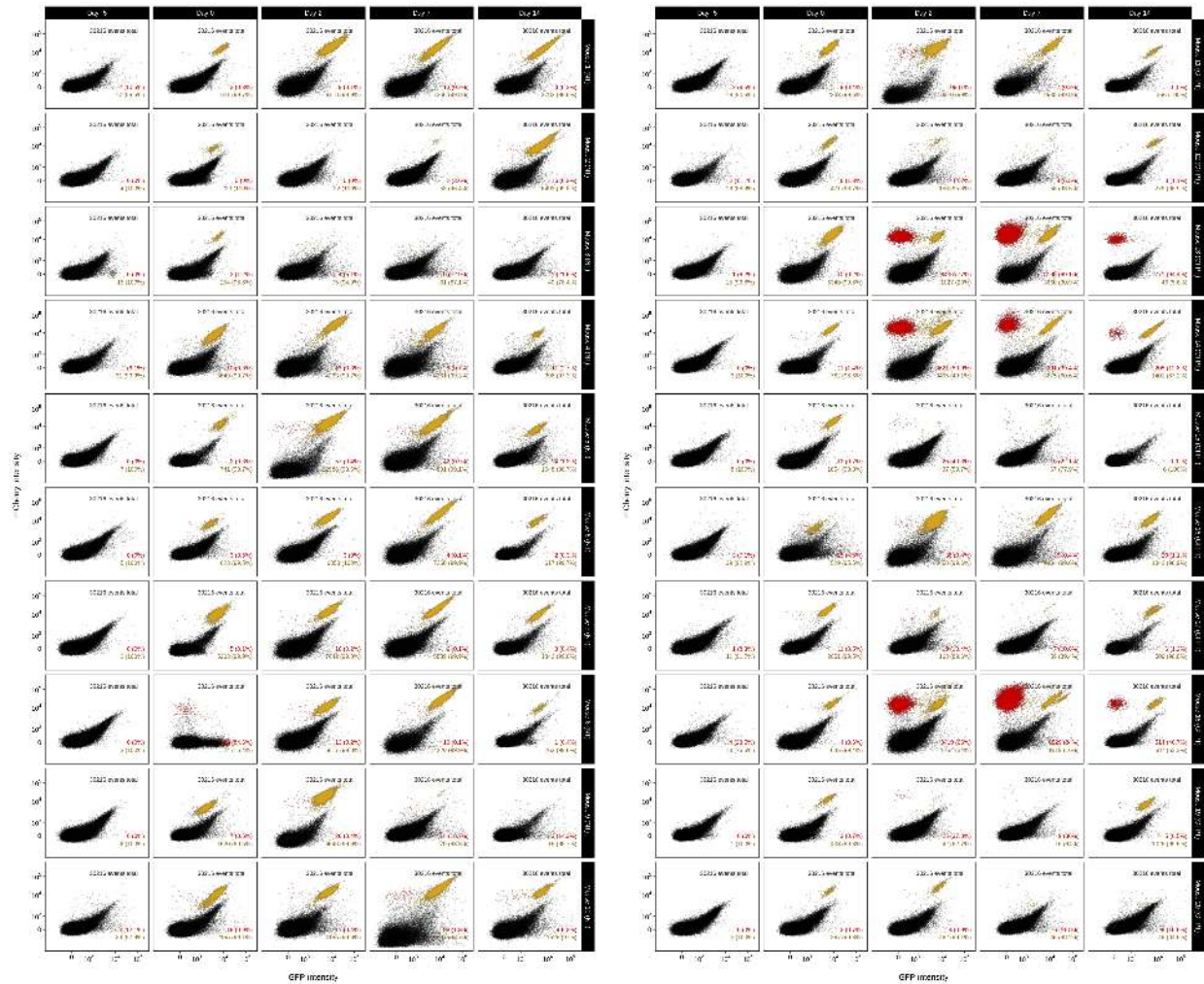


Figure S13. Flow cytometry plots of fecal samples for *in vivo* targeting of double-marked *E. coli* for all mice at all timepoints. Mice ($n = 10$ per group) were given either NT M13 (left) or GFPT M13 (right). Day -5, before engrafting *E. coli*; Day 0, after engraftment with double-marked GFP+ mCherry+ *E. coli*; Day -2, post phage and carbenicillin treatment; Day 7, one week post-phage and carbenicillin; Day -14, one week after removing carbenicillin from drinking water. Based on visual inspection, sample from Mouse 8 Day 0 was omitted from analyses.

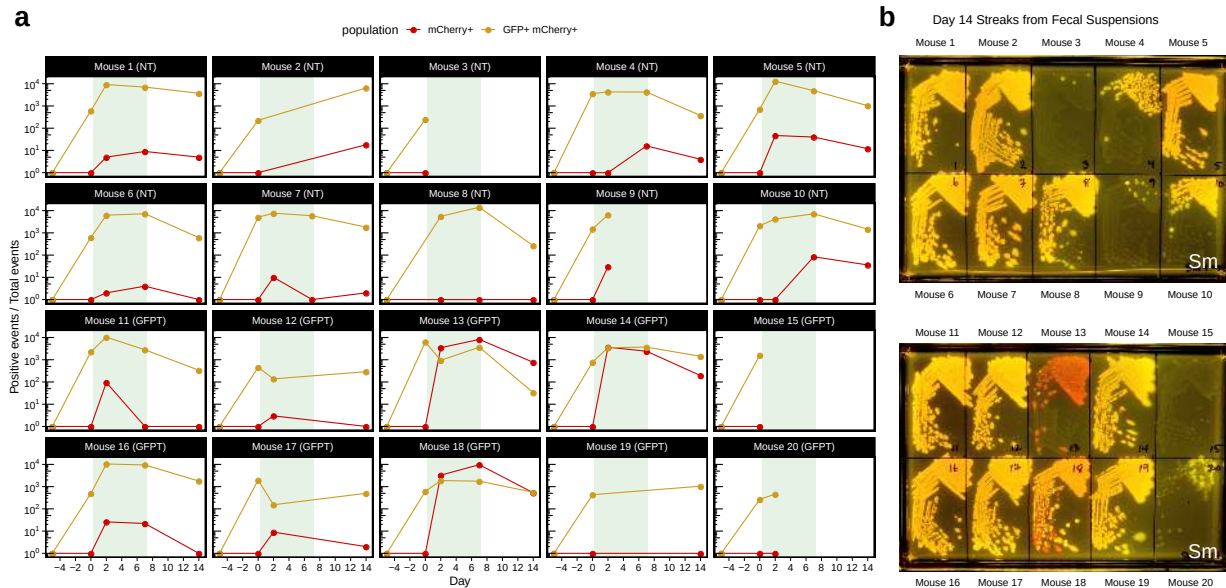


Figure S14. Doubly GFP+ mCherry+ and singly mCherry+ events by flow cytometry in fecal samples over time for individual mice in colonized with the double-marked strain under NT or GFPT conditions. (a) For each mouse, the number of doubly GFP+ mCherry+ events on Day -5 (before *E. coli* engraftment) was used to subtract GFP+ mCherry+ background for all subsequent timepoints, and the number of singly mCherry+ events on Day 0 (before phage treatment) was used to subtract mCherry+ background from all subsequent timepoints. Shaded green area indicates duration of carbenicillin treatment. Timepoints were excluded when both doubly GFP+ mCherry+ and singly mCherry+ events were below background thresholds, calculated as the respective highest observed background multiplied by a factor of 3. **(b)** Culture on LB with streptomycin from Day 14 fecal suspensions of mice treated with NT M13 (M1 to M10) and GFPT M13 (M11 to M20). Lack of fluorescent *E. coli* in fecal samples indicates eradication by carbenicillin where phage infection leading to colonization by Carb^R *E. coli* did not occur during the treatment phase.

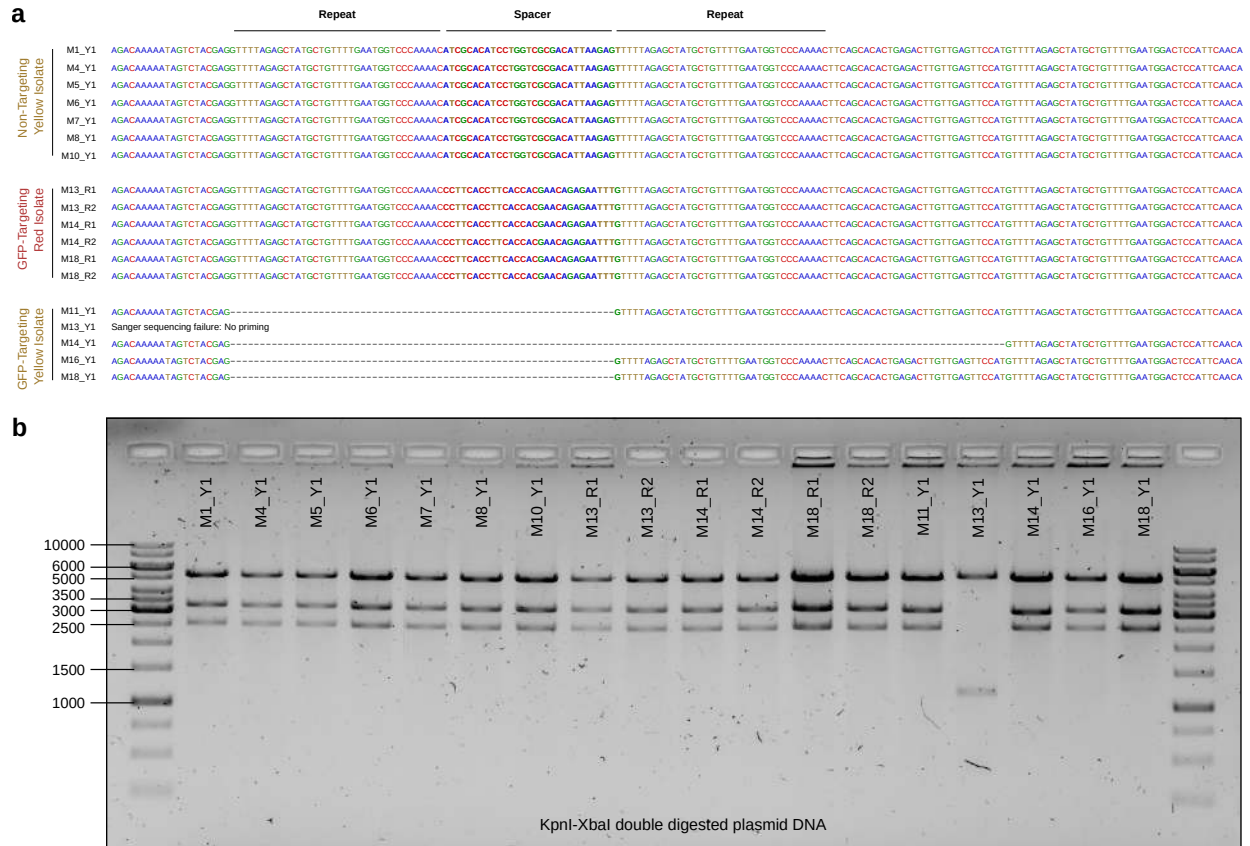


Figure S15. *E. coli* isolates that remain double positive (GFP+ mCherry+) in fecal samples of mice treated with GFP-targeting M13 harbour CRISPR-Cas9 phagemids that exhibit loss of DNA. (a) Sanger sequencing results confirm the expected spacer present in phagemid DNA extracted from fluorescent yellow isolates (Y1) colonizing NT mice (M1, M4, M5, M6, M7, M8, M10) and fluorescent red isolates (R1 and R2) colonizing GFPT mice (M13, M14, M18). In contrast, 4 of the 5 fluorescent yellow isolates colonizing GFPT mice (M11, M13, M14, M16, M18) were confirmed to have lost the spacer. No Sanger sequence data was obtained for the last isolate (M13) with report for failing being No Priming, suggesting loss of a larger fragment from the phagemid. **(b)** Diagnostic digest of CRISPR-Cas9 phagemid DNA confirms sizeable loss of phagemid DNA for the phagemid extracted from M13 Y1. Expected fragment sizes from KpnI-XbaI double digest: 5289, 3285, and 2573 bp.

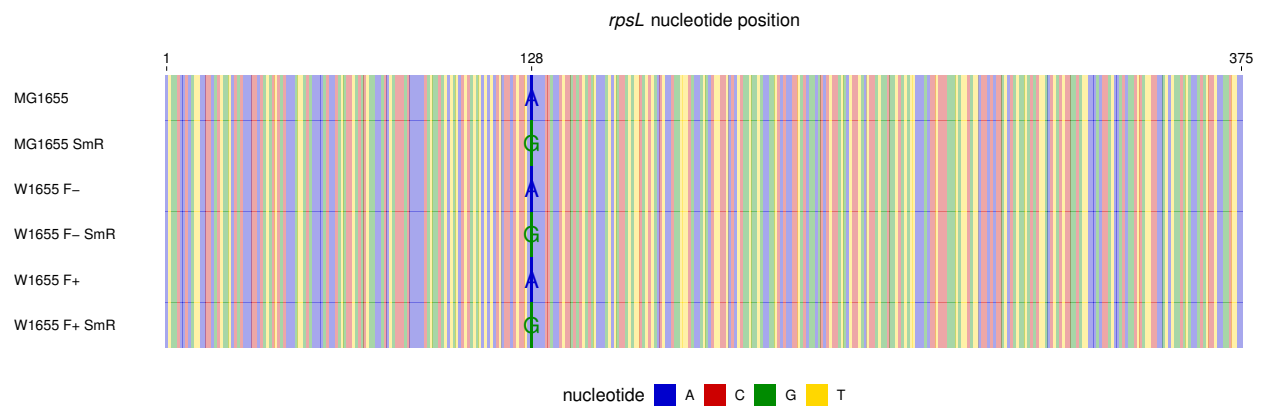


Figure S16. Confirmation of *rpsL*-Sm^R alleles by Sanger sequencing. The *rpsL* gene sequence is identical between *E. coli* MG1655, W1655 F⁻, and W1655 F⁺. Lambda Red recombineering was used to generate Sm^R derivatives of W1655 F⁻ and W1655 F⁺ strains with identical alleles to MG1655 Sm^R, a spontaneous resistant mutant; all 3 were confirmed to have an A to G mutation at nucleotide 128 resulting in Lys42Arg.

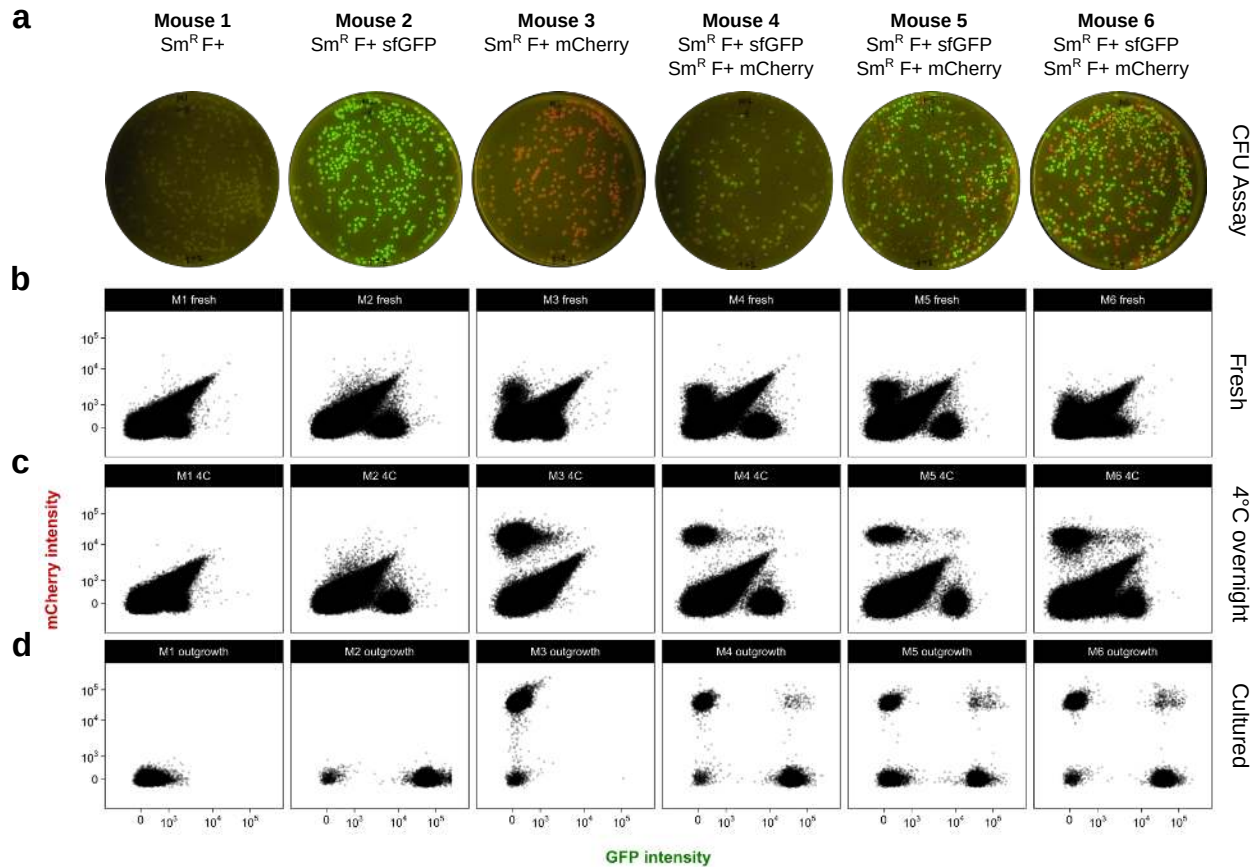


Figure S17. Quantification of fluorescent *E. coli* in mouse fecal pellets by flow cytometry improves with overnight incubation of fecal suspensions at 4 °C. (a) Culture on LB streptomycin of fecal suspensions from streptomycin-treated mice colonized with non-fluorescent Sm^R *E. coli* W1655 F+ (Mouse 1), the GFP-marked (Mouse 2) or mCherry-marked derivative (Mouse 3), or both fluorescent strains (Mouse 4, 5, and 6). Flow cytometry was performed on fecal suspensions: (b) immediately after collecting, (c) overnight incubation at 4 °C, or (d) after inoculation in media and overnight culture.

Table S1. 16S rRNA gene sequencing indexing PCR primer sequences.

Name	PrimerSeq	Origin	IndexName	IndexSeq
F1_MetaIndex	AATGATACGGCGACCACCGAGATCTACACTATAGCCTTCGTGGCAGCGTC	TruSeq i5	D501	TATAGCCT
F2_MetaIndex	AATGATACGGCGACCACCGAGATCTACACATAGAGGCTCGTGGCAGCGTC	TruSeq i5	D502	ATAGAGGC
F3_MetaIndex	AATGATACGGCGACCACCGAGATCTACACCTATCCTTCGTGGCAGCGTC	TruSeq i5	D503	CCTATCCT
F4_MetaIndex	AATGATACGGCGACCACCGAGATCTACACGGCTCTGATCGTGGCAGCGTC	TruSeq i5	D504	GGCTCTGA
F5_MetaIndex	AATGATACGGCGACCACCGAGATCTACACAGCGAAGTCTGGCAGCGTC	TruSeq i5	D505	AGGCGAAG
F6_MetaIndex	AATGATACGGCGACCACCGAGATCTACACTAATCTTATCGTGGCAGCGTC	TruSeq i5	D506	TAATCTTA
F7_MetaIndex	AATGATACGGCGACCACCGAGATCTACACAGGACGTTCTGGCAGCGTC	TruSeq i5	D507	CAGGACGT
F8_MetaIndex	AATGATACGGCGACCACCGAGATCTACACGTAAGTCTGGCAGCGTC	TruSeq i5	D508	GTACTGAC
F9_MetaIndex	AATGATACGGCGACCACCGAGATCTACACTGAACCTTCGTGGCAGCGTC	TruSeq Amplicon	A501	TGAACCTT
F10_MetaIndex	AATGATACGGCGACCACCGAGATCTACACTAGATCGTGGCAGCGTC	Nextera i5	N501	TAGATCGC
F11_MetaIndex	AATGATACGGCGACCACCGAGATCTACACTCTCTTCGTGGCAGCGTC	Nextera i5	N502	CTCTCTAT
F12_MetaIndex	AATGATACGGCGACCACCGAGATCTACACTATCCTTCGTGGCAGCGTC	Nextera i5	N503	TATCCTCT
F13_MetaIndex	AATGATACGGCGACCACCGAGATCTACACAGATAGTCTGGCAGCGTC	Nextera i5	N504	AGAGTAGA
F14_MetaIndex	AATGATACGGCGACCACCGAGATCTACACGTAAGGAGTCTGGCAGCGTC	Nextera i5	N505	GTAGGGAG
F15_MetaIndex	AATGATACGGCGACCACCGAGATCTACACATGATCTGGCAGCGTC	Nextera i5	N506	ACTGATA
F16_MetaIndex	AATGATACGGCGACCACCGAGATCTACACAAGGATATCTGGCAGCGTC	Nextera i5	N507	AAGGAGTA
R13_MetaIndex	CAAGCAGAAGACGGCATAACGAGATTCGTGGTCTCGTGGGCTCGG	TruSeq Amplicon	A701	ATCAGCAC
R14_MetaIndex	CAAGCAGAAGACGGCATAACGAGATCGAGTAATGTCTCGTGGGCTCGG	TruSeq i7	D701	ATTACTCG
R15_MetaIndex	CAAGCAGAAGACGGCATAACGAGATTCCTGGGAGTCTCGTGGGCTCGG	TruSeq i7	D702	TCCGGAGA
R16_MetaIndex	CAAGCAGAAGACGGCATAACGAGATAAAGAGGGTCTCGTGGGCTCGG	TruSeq i7	D703	CGCTCATT
R17_MetaIndex	CAAGCAGAAGACGGCATAACGAGATGGAATCTCGTGGGCTCGG	TruSeq i7	D704	GAGATTC
R18_MetaIndex	CAAGCAGAAGACGGCATAACGAGATTTCTGAATGTCTCGTGGGCTCGG	TruSeq i7	D705	ATTGAGAA
R19_MetaIndex	CAAGCAGAAGACGGCATAACGAGATACGAATTCGTGGGCTCGG	TruSeq i7	D706	GAATTCGT
R20_MetaIndex	CAAGCAGAAGACGGCATAACGAGATAGCTTCAGGTCTCGTGGGCTCGG	TruSeq i7	D707	CTGAAGCT
R21_MetaIndex	CAAGCAGAAGACGGCATAACGAGATGCGCATTAGTCTCGTGGGCTCGG	TruSeq i7	D708	TAATCGGC
R22_MetaIndex	CAAGCAGAAGACGGCATAACGAGATCATAGCCGGTCTCGTGGGCTCGG	TruSeq i7	D709	CGGCTATG
R23_MetaIndex	CAAGCAGAAGACGGCATAACGAGATTCGGGAGTCTCGTGGGCTCGG	TruSeq i7	D710	TCCGGCAA
R24_MetaIndex	CAAGCAGAAGACGGCATAACGAGATGCGCGAGGCTCTCGTGGGCTCGG	TruSeq i7	D711	TCTGGCC
R1_MetaIndex	CAAGCAGAAGACGGCATAACGAGATTCGCTTAGTCTCGTGGGCTCGG	Nextera i7	N701	TAGGGCGA
R2_MetaIndex	CAAGCAGAAGACGGCATAACGAGATCTAGTACGGTCTCGTGGGCTCGG	Nextera i7	N702	CCTACTAG
R3_MetaIndex	CAAGCAGAAGACGGCATAACGAGATTTCTGCTCTCTGGGCTCGG	Nextera i7	N703	AGCAGAA
R4_MetaIndex	CAAGCAGAAGACGGCATAACGAGATGCTCAGGAGTCTCGTGGGCTCGG	Nextera i7	N704	TCTGAGC
R5_MetaIndex	CAAGCAGAAGACGGCATAACGAGATAGGAGTCTCGTGGGCTCGG	Nextera i7	N705	GGACTCCT
R6_MetaIndex	CAAGCAGAAGACGGCATAACGAGATCATGCTAGTCTCGTGGGCTCGG	Nextera i7	N706	TAGGCATG
R7_MetaIndex	CAAGCAGAAGACGGCATAACGAGATGATAGAGGTTCTCGTGGGCTCGG	Nextera i7	N707	CTCTCTAC
R8_MetaIndex	CAAGCAGAAGACGGCATAACGAGATCCTCTCTGGTCTCGTGGGCTCGG	Nextera i7	N708	CAGAGAGG
R25_MetaIndex	CAAGCAGAAGACGGCATAACGAGATCTATCGCTCTCGTGGGCTCGG	TruSeq i7	D712	AGCAGATG
R10_MetaIndex	CAAGCAGAAGACGGCATAACGAGATCAGCTCGTCTCGTGGGCTCGG	Nextera i7	N710	CGAGGCTG
R11_MetaIndex	CAAGCAGAAGACGGCATAACGAGATTCCTCTCTGGTCTCGTGGGCTCGG	Nextera i7	N711	AAGAGGCA
R12_MetaIndex	CAAGCAGAAGACGGCATAACGAGATTCCTACTCTCGTGGGCTCGG	Nextera i7	N712	GTAGAGGA

Table S2. 16S rRNA gene sequencing sample metadata.

Sample_ID	Index_ID	Index	Index2_ID	Index2	Sample_Well	Specimen	Timepoint	Sample_Type	Mouse	Day	chem_administration	host_body_product
exp11_M1_Prev-Sm	D706	GAAATTCG	D505	AGGAGGAG	A7	M1	P	Pre-Sm	Mouse	M1	-5	stool
exp11_M1_Prev-Sm	D704	CGATGATG	D505	ATAGAGG	F5	M10	P	Pre-Sm	Mouse	M1	-5	stool
exp11_M1_Prev-Sm	D709	CGGATGAT	D501	TATAGCTT	B10	M11	P	Pre-Sm	Mouse	M1	-5	stool
exp11_M1_Prev-Sm	D704	ATTACTCG	D504	AGGATGCT	B2	M12	P	Pre-Sm	Mouse	M1	-5	stool
exp11_M1_Prev-Sm	D707	CTGAAGCT	D503	CCCTATCT	C8	M13	P	Pre-Sm	Mouse	M1	-5	stool
exp11_M1_Prev-Sm	D702	TCGGGAGA	D501	TATAGCTC	B3	M14	P	Pre-Sm	Mouse	M1	-5	stool
exp11_M1_Prev-Sm	D709	CGGATGAT	D505	AGGCGAAG	R10	M15	P	Pre-Sm	Mouse	M1	-5	stool
exp11_M1_Prev-Sm	D701	ATTACTCG	D506	ACTCCTA	G2	M16	P	Pre-Sm	Mouse	M1	-5	stool
exp11_M1_Prev-Sm	D708	TAAATGCG	D506	TAACTCTA	F9	M17	P	Pre-Sm	Mouse	M1	-5	stool
exp11_M1_Prev-Sm	D704	ATTACTCG	D501	TAGACTCT	B1	M18	P	Pre-Sm	Mouse	M1	-5	stool
exp11_M1_Prev-Sm	D702	TCGGGAGA	D505	AGGCGAAG	B3	M19	P	Pre-Sm	Mouse	M1	-5	stool
exp11_M1_Prev-Sm	D704	GAAATTCG	D506	AGGATGCT	C5	M2	P	Pre-Sm	Mouse	M1	-5	stool
exp11_M1_Prev-Sm	D703	CGCTCAT	D503	TATCCTCT	D4	M20	P	Pre-Sm	Mouse	M1	-5	stool
exp11_M1_Prev-Sm	D702	TCGGGAGA	D508	GTACTGAC	B3	M21	P	Pre-Sm	Mouse	M1	-5	stool
exp11_M1_Prev-Sm	D701	ATTACTCG	D507	CAGGACT	H1	M22	P	Pre-Sm	Mouse	M1	-5	stool
exp11_M1_Prev-Sm	D704	GAAATTCG	D505	AGGCGAAG	E5	M23	P	Pre-Sm	Mouse	M1	-5	stool
exp11_M1_Prev-Sm	D704	GAAATTCG	D501	TGAACTCT	A5	M24	P	Pre-Sm	Mouse	M1	-5	stool
exp11_M1_Prev-Sm	D701	ATTACTCG	D505	GTAAAGG	F2	M4	P	Pre-Sm	Mouse	M1	-5	stool
exp11_M1_Prev-Sm	D706	GAAATTCG	D507	AGAGTGA	G7	M5	P	Pre-Sm	Mouse	M1	-5	stool
exp11_M1_Prev-Sm	D705	ATTCAAGA	D502	CCCTCAT	C4	M6	P	Pre-Sm	Mouse	M1	-5	stool
exp11_M1_Prev-Sm	D704	GAAATTCG	D506	TAACTCTA	F5	M7	P	Pre-Sm	Mouse	M1	-5	stool
exp11_M1_Prev-Sm	D705	ATTCAAGA	D501	TGAACTCT	A6	M8	P	Pre-Sm	Mouse	M1	-5	stool
exp11_M1_Prev-Sm	D707	CTGAAGCT	D505	AGGCGAAG	E8	M9	P	Pre-Sm	Mouse	M1	-5	stool
exp11_M1_Prev-Col	D708	TAAATGCG	D501	TATAGCTT	A9	M1	P	Post-Sm (Pre-Col)	Mouse	M1	-4	Streptomycin
exp11_M1_Prev-Col	D701	ATTACTCG	D501	AGGATGCT	B1	M10	P	Post-Sm (Pre-Col)	Mouse	M1	-4	Streptomycin
exp11_M1_Prev-Col	D702	TCGGGAGA	D503	CCCTATCT	C3	M11	P	Post-Sm (Pre-Col)	Mouse	M1	-4	Streptomycin
exp11_M1_Prev-Col	D706	GAAATTCG	D501	TGAACTCT	A7	M12	P	Post-Sm (Pre-Col)	Mouse	M1	-4	Streptomycin
exp11_M1_Prev-Col	D701	ATTACTCG	D507	AGAGTGA	G2	M13	P	Post-Sm (Pre-Col)	Mouse	M1	-4	Streptomycin
exp11_M1_Prev-Col	D703	CGCTCAT	D504	AGAGTGA	E4	M14	P	Post-Sm (Pre-Col)	Mouse	M1	-4	Streptomycin
exp11_M1_Prev-Col	D703	CGCTCAT	D505	AGGCGAAG	E4	M15	P	Post-Sm (Pre-Col)	Mouse	M1	-4	Streptomycin
exp11_M1_Prev-Col	D701	ATTACTCG	D504	AGAGTGA	E1	M16	P	Post-Sm (Pre-Col)	Mouse	M1	-4	Streptomycin
exp11_M1_Prev-Col	D701	ATTACTCG	D502	TATAGCTT	A1	M17	P	Post-Sm (Pre-Col)	Mouse	M1	-4	Streptomycin
exp11_M1_Prev-Col	D703	CGCTCAT	D503	CAGGACT	H1	M18	P	Post-Sm (Pre-Col)	Mouse	M1	-4	Streptomycin
exp11_M1_Prev-Col	D702	TCGGGAGA	D501	TATAGCTT	A3	M19	P	Post-Sm (Pre-Col)	Mouse	M1	-4	Streptomycin
exp11_M1_Prev-Col	D711	TCGGGAGA	D501	TATAGCTT	B1	M2	P	Post-Sm (Pre-Col)	Mouse	M1	-4	Streptomycin
exp11_M1_Prev-Col	D711	TCGGGAGA	D501	TATAGCTT	A1	M20	P	Post-Sm (Pre-Col)	Mouse	M1	-4	Streptomycin
exp11_M1_Prev-Col	D704	GAAATTCG	D503	CCCTATCT	C5	M21	P	Post-Sm (Pre-Col)	Mouse	M1	-4	Streptomycin
exp11_M1_Prev-Col	D701	ATTACTCG	D503	CCCTATCT	C2	M22	P	Post-Sm (Pre-Col)	Mouse	M1	-4	Streptomycin
exp11_M1_Prev-Col	D709	CGGATGAT	D508	GTACTGAC	H10	M23	P	Post-Sm (Pre-Col)	Mouse	M1	-4	Streptomycin
exp11_M1_Prev-Col	D711	TCGGGAGA	D504	GGCTCTGA	D12	M24	P	Post-Sm (Pre-Col)	Mouse	M1	-4	Streptomycin
exp11_M1_Prev-Col	D709	CGGATGAT	D504	GGCTCTGA	D10	M3	P	Post-Sm (Pre-Col)	Mouse	M1	-4	Streptomycin
exp11_M1_Prev-Col	D706	GAAATTCG	D502	CTCCTCAT	C7	M4	P	Post-Sm (Pre-Col)	Mouse	M1	-4	Streptomycin
exp11_M1_Prev-Col	D702	TCGGGAGA	D502	ATAGAGG	B4	M5	P	Post-Sm (Pre-Col)	Mouse	M1	-4	Streptomycin
exp11_M1_Prev-Col	A701	ATTACTCG	D502	GTAAAGG	F1	M6	P	Post-Sm (Pre-Col)	Mouse	M1	-4	Streptomycin
exp11_M1_Prev-Col	D708	TAAATGCG	D507	AGAGTGA	G9	M7	P	Post-Sm (Pre-Col)	Mouse	M1	-4	Streptomycin
exp11_M1_Prev-Col	D704	GAAATTCG	D504	AGGATGCT	E5	M8	P	Post-Sm (Pre-Col)	Mouse	M1	-4	Streptomycin
exp11_M1_Prev-Col	D703	CGCTCAT	D503	CCCTATCT	C4	M9	P	Post-Sm (Pre-Col)	Mouse	M1	-4	Streptomycin
exp11_M1_T-2	D704	GAAATTCG	D507	AGAGTGA	G5	M1	P	Post-Col	Mouse	M1	-2	Streptomycin
exp11_M1_T-2	D707	CTGAAGCT	D502	AGGCGAAG	E8	M10	P	Post-Col	Mouse	M1	-2	Streptomycin
exp11_M1_T-2	D701	ATTACTCG	D502	ATAGAGG	B2	M11	P	Post-Col	Mouse	M1	-2	Streptomycin
exp11_M1_T-2	D704	GAAATTCG	D502	CTCCTCAT	C7	M12	P	Post-Col	Mouse	M1	-2	Streptomycin
exp11_M1_T-2	D704	GAAATTCG	D508	GTACTGAC	H5	M13	P	Post-Col	Mouse	M1	-2	Streptomycin
exp11_M1_T-2	D710	TCGGGAGA	D505	AGGCGAAG	E1	M14	P	Post-Col	Mouse	M1	-2	Streptomycin
exp11_M1_T-2	D706	TCGGGAGA	D507	AGGCGAAG	E3	M15	P	Post-Col	Mouse	M1	-2	Streptomycin
exp11_M1_T-2	D710	TCGGGAGA	D507	AGGCGAAG	G11	M16	P	Post-Col	Mouse	M1	-2	Streptomycin
exp11_M1_T-2	D706	GAAATTCG	D504	GGCTCTGA	D7	M17	P	Post-Col	Mouse	M1	-2	Streptomycin
exp11_M1_T-2	D704	GAAATTCG	D503	CCCTATCT	D7	M18	P	Post-Col	Mouse	M1	-2	Streptomycin
exp11_M1_T-2	D704	GAAATTCG	D502	ATAGAGG	B5	M19	P	Post-Col	Mouse	M1	-2	Streptomycin
exp11_M1_T-2	D701	ATTACTCG	D501	TGAACTCT	A2	M2	P	Post-Col	Mouse	M1	-2	Streptomycin
exp11_M1_T-2	D701	ATTACTCG	D503	CCCTATCT	D2	M20	P	Post-Col	Mouse	M1	-2	Streptomycin
exp11_M1_T-2	D706	GAAATTCG	D501	TATAGCTT	A7	M21	P	Post-Col	Mouse	M1	-2	Streptomycin
exp11_M1_T-2	D704	GAAATTCG	D503	CCCTATCT	D5	M22	P	Post-Col	Mouse	M1	-2	Streptomycin
exp11_M1_T-2	D708	TAAATGCG	D502	ATAGAGG	B9	M23	P	Post-Col	Mouse	M1	-2	Streptomycin
exp11_M1_T-2	D701	ATTACTCG	D503	TATCCTCT	D1	M24	P	Post-Col	Mouse	M1	-2	Streptomycin
exp11_M1_T-2	D708	TAAATGCG	D508	GTACTGAC	H9	M3	P	Post-Col	Mouse	M1	-2	Streptomycin
exp11_M1_T-2	D703	CGCTCAT	D501	TGAACTCT	A4	M4	P	Post-Col	Mouse	M1	-2	Streptomycin
exp11_M1_T-2	A701	ATTACTCG	D501	TATAGCTT	A1	M5	P	Post-Col	Mouse	M1	-2	Streptomycin
exp11_M1_T-2	D702	TCGGGAGA	D502	CTCCTCAT	C7	M6	P	Post-Col	Mouse	M1	-2	Streptomycin
exp11_M1_T-2	A701	ATTACTCG	D501	AGAGTGA	G1	M7	P	Post-Col	Mouse	M1	-2	Streptomycin
exp11_M1_T-2	D704	GAAATTCG	D504	AGGATGCT	E5	M8	P	Post-Col	Mouse	M1	-2	Streptomycin
exp11_M1_T-2	D706	GAAATTCG	D503	CCCTATCT	C7	M9	P	Post-Col	Mouse	M1	-2	Streptomycin
exp11_M1_T-2	D705	ATTCAAGA	D502	ATAGAGG	B6	M1	P	Post-Col	Mouse	M1	-2	Streptomycin
exp11_M1_T-2	D707	CTGAAGCT	D504	AGGCGAAG	E8	M10	P	Post-Col	Mouse	M1	-2	Streptomycin
exp11_M1_T-2	D702	TCGGGAGA	D506	TAACTCTA	F3	M11	T0	Mouse	M1	0	Streptomycin	
exp11_M1_T-2	D702	TCGGGAGA	D501	TGAACTCT	A3	M12	T0	Mouse	M1	0	Streptomycin	
exp11_M1_T-2	D706	GAAATTCG	D508	GTACTGAC	H7	M13	T0	Mouse	M1	0	Streptomycin	
exp11_M1_T-2	D711	TCGGGAGA	D503	CCCTATCT	C12	M14	T0	Mouse	M1	0	Streptomycin	
exp11_M1_T-2	D705	ATTCAAGA	D505	TAACTCTA	F2	M15	T0	Mouse	M1	0	Streptomycin	
exp11_M1_T-2	D705	ATTCAAGA	D508	GTACTGAC	H6	M16	T0	Mouse	M1	0	Streptomycin	
exp11_M1_T-2	D711	TCGGGAGA	D502	ATAGAGG	B1	M17	T0	Mouse	M1	0	Streptomycin	
exp11_M1_T-2	D708	TAAATGCG	D504	GGCTCTGA	D9	M19	T0	Mouse	M1	0	Streptomycin	
exp11_M1_T-2	D706	GAAATTCG	D501	TATAGCTT	B7	M20	T0	Mouse	M1	0	Streptomycin	
exp11_M1_T-2	D703	CGCTCAT	D506	ACTCCTA	G4	M20	T0	Mouse	M1	0	Streptomycin	
exp11_M1_T-2	D701	ATTACTCG	D505	AGGCGAAG	E2	M21	T0	Mouse	M1	0	Streptomycin	
exp11_M1_T-2	D703	CGCTCAT	D501	TATAGCTT	A4	M22	T0	Mouse	M1	0	Streptomycin	
exp11_M1_T-2	D707	CTGAAGCT	D504	GGCTCTGA	D8	M23	T0	Mouse	M1	0	Streptomycin	
exp11_M1_T-2	D710	TCGGGAGA	D506	GTACTGAC	H11	M24	T0	Mouse	M1	0	Streptomycin	
exp11_M1_T-2	D710	TCGGGAGA	D501	TATAGCTT	A3	M2	T0	Mouse	M1	0	Streptomycin	
exp11_M1_T-2	D701	ATTACTCG	D508	GTACTGAC	H1	M3	T0	Mouse	M1	0	Streptomycin	
exp11_M1_T-2	D706	GAAATTCG	D507	CAGGACT	H7	M4	T0	Mouse	M1	0	Streptomycin	
exp11_M1_T-2	D709	CGGATGAT	D502	GTACTGAC	B10	M5	T0	Mouse	M1	0	Streptomycin	
exp11_M1_T-2	D707	CTGAAGCT	D503	CCCTATCT	D8	M6	T0	Mouse	M1	0	Streptomycin	
exp11_M1_T-2	D704	GAAATTCG	D501	TATAGCTT	A7	M7	T0	Mouse	M1	0	Streptomycin	
exp11_M1_T-2	D702	TCGGGAGA	D503	CCCTATCT	C11	M8	T0	Mouse	M1	0	Streptomycin	
exp11_M1_T-2	D703	CGCTCAT	D501	TATAGCTT	A4	M9	T0	Mouse	M1	0	Streptomycin	
exp11_M1_T1	D705	ATTCAAGA	D507	AGAGTGA	G6	M1	T1	Mouse	M1	1	Streptomycin, Carbencillin	
exp11_M1_T1	D707	CTGAAGCT	D501	TGAACTCT	A6	M10	T1	Mouse	M1	1	Streptomycin, Carbencillin	
exp11_M1_T1	D701	ATTACTCG	D501	TATAGCTT	A2	M11	T1	Mouse	M1	1	Streptomycin, Carbencillin	
exp11_M1_T1	D701	ATTACTCG	D507	CAGGACT	H2	M12	T1	Mouse	M1	1	Streptomycin, Carbencillin	
exp11_M1_T1	D705	ATTCAAGA	D506	TAACTCTA	F6	M13	T1	Mouse	M1	1	Streptomycin, Carbencillin	
exp11_M1_T1	D710	TCGGGAGA	D504	GGCTCTGA	D11	M14	T1	Mouse	M1	1	Streptomycin, Carbencillin	
exp11_M1_T1	D703	CGCTCAT	D504	GGCTCTGA	D4	M15	T1	Mouse	M1	1	Streptomycin, Carbencillin	
exp11_M1_T1	D701	ATTACTCG	D501	TATAGCTT	A2	M16	T1	Mouse	M1	1	Streptomycin, Carbencillin	
exp11_M1_T1	A701	ATTACTCG	D503	CCCTATCT	C11	M17	T1	Mouse	M1	1	Streptomycin, Carbencillin	
exp11_M1_T1	D707	CTGAAGCT	D501	TATAGCTT	A8	M18	T1	Mouse	M1	1	Streptomycin, Carbencillin	
exp11_M1_T1	D705	ATTCAAGA	D504	GGCTCTGA	D6	M19	T1	Mouse	M1	1	Streptomycin, Carbencillin	
exp11_M1_T1	D710	TCGGGAGA	D508	GTACTGAC	H11	M2	T1	Mouse	M1	1	Streptomycin, Carbencillin	
exp11_M1_T1	D710	TCGGGAGA	D501	TATAGCTT	A3	M20	T1	Mouse	M1	1	Streptomycin, Carbencillin	
exp11_M1_T1	D703	CGCTCAT	D508	GTACTGAC	H4	M21	T1	Mouse	M1	1	Streptomycin, Carbencillin	
exp11_M1_T1	D704	GAAATTCG	D507	CAGGACT	H5	M22	T1	Mouse	M1	1	Streptomycin, Carbencillin	
exp11_M1_T1	A701	ATTACTCG	D505	AGGCGAAG	E1	M23	T1	Mouse	M1	1	Streptomycin, Carbencillin	
exp11_M1_T1	D702	TCGGGAGA	D503	TATCCTCT	D3	M24	T1	Mouse	M1	1	Streptomycin, Carbencillin	
exp11_M1_T1	D708	TAAATGCG	D505	GTAAAGG	F8	M3	T1	Mouse	M1	1	Streptomycin, Carbencillin	
exp11_M1_T1	D707	CTGAAGCT	D505	GTAAAGG	F8	M4	T1	Mouse	M1	1	Streptomycin, Carbencillin	
exp11_M1_T1	D709	CGGATGAT	D503	CCCTATCT	C10	M5	T1	Mouse	M1	1	Streptomycin, Carbencillin	
exp11_M1_T1	D702	TCGGGAGA	D501	CCCTATCT	C3	M6	T1	Mouse	M1	1	Streptomycin, Carbencillin	
exp11_M1_T1	D707	CTGAAGCT	D502	ATAGAGG	B2	M7	T1	Mouse	M1	1	Streptomycin, Carbencillin	

Word Count

File: main.tex

Encoding: ascii

Sum count: 6438

Words in text: 5083

Words in headers: 40

Words outside text (captions, etc.): 1315

Number of headers: 11

Number of floats/tables/figures: 5

Number of math inlines: 0

Number of math displayed: 0

Subcounts:

text+headers+captions (#headers/#floats/#inlines/#displayed)

1+0+0 (0/0/0/0) Subsection

932+1+0 (1/0/0/0) Section: Introduction

0+1+0 (1/0/0/0) Section: Results

1182+12+337 (1/1/0/0) Subsection: Phage M13 can be used to deliver DNA to *Ecoli* in the gut

975+5+431 (1/2/0/0) Subsection: M13 carrying CRISPR-Cas9 can target *Ecoli* *invitro*

446+6+307 (1/1/0/0) Subsection: Sequence-specific depletion of *Ecoli* *invivo* using M13-delivered CRISPR-Cas9

550+6+240 (1/1/0/0) Subsection: M13-delivered CRISPR-Cas9 can induce chromosomal deletions *invivo*

610+1+0 (1/0/0/0) Section: Discussion

130+1+0 (1/0/0/0) Section: Acknowledgments

103+2+0 (1/0/0/0) Section: Author Contributions

115+1+0 (1/0/0/0) Section: Funding

39+4+0 (1/0/0/0) Section: Conflict of Interest Statement